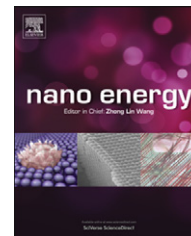




Available online at [www.sciencedirect.com](http://www.sciencedirect.com)

SciVerse ScienceDirect

journal homepage: [www.elsevier.com/locate/nanoenergy](http://www.elsevier.com/locate/nanoenergy)



## REVIEW

# Nanostructured carbon for energy storage and conversion

Stephanie L. Candelaria<sup>a</sup>, Yuyan Shao<sup>b</sup>, Wei Zhou<sup>c,d</sup>, Xiaolin Li<sup>b</sup>, Jie Xiao<sup>b</sup>, Ji-Guang Zhang<sup>b</sup>, Yong Wang<sup>b</sup>, Jun Liu<sup>b,\*</sup>, Jinghong Li<sup>c,d,\*\*</sup>, Guozhong Cao<sup>a,\*</sup>

<sup>a</sup>Department of Materials Science and Engineering, University of Washington, Seattle, WA 98195, USA

<sup>b</sup>Pacific Northwest National Laboratory, Richland, WA 99352, USA

<sup>c</sup>Department of Chemistry, Beijing Key Laboratory for Microanalytical Methods and Instrumentation, Tsinghua University, Beijing 100084, China

<sup>d</sup>Key Laboratory of Bioorganic Phosphorus Chemistry & Chemical Biology, Tsinghua University, Beijing, China

Available online 23 December 2011

### KEYWORDS

Porous carbon;  
Carbon nanotubes;  
Graphene;  
Supercapacitor;  
Electrocatalyst;  
Lithium battery

### Abstract

Carbon materials have been playing a significant role in the development of alternative clean and sustainable energy technologies. This review article summarizes the recent research progress on the synthesis of nanostructured carbon and its application in energy storage and conversion. In particular, we will systematically discuss the synthesis and applications of nanoporous carbon as electrodes for supercapacitors and electrodes in lithium-ion batteries, and the development of nanoporous media for methane gas storage, coherent nanocomposites for hydrogen storage, electrocatalysts and catalyst supports for fuel cells, new porous carbon for lithium-sulfur batteries, and porous carbon for lithium-oxygen batteries. The common challenges in developing simple, scalable, and environmentally friendly synthetic and manufacturing processes, in controlling the nanoscale and high level structures and functions, and in integrating such materials with suitable device architectures are reviewed. Possible new directions to overcome the current limitations on the performance are discussed.

© 2011 Elsevier Ltd. All rights reserved.

## Introduction

Carbon is one of the most abundant elements on the Earth, and plays a critical role in the bio- and ecosystems as we know them today. For thousands of years, carbon has also been a source of energy, and human history is closely associated with the struggle to extract and utilize power from carbon materials. The technologies that have enabled our modern society such as automobiles, airplanes, computers, lasers, and portable electronics, just to name a few,

\*Corresponding authors.

\*\*Corresponding author at: Department of Chemistry, Beijing Key Laboratory for Microanalytical Methods and Instrumentation, Tsinghua University, Beijing 100084, China.

*E-mail addresses:* jun.liu@pnl.gov (J. Liu),  
jhli@mail.tsinghua.edu.cn (J. Li),  
gzcao@u.washington.edu, gzcao@uw.edu (G. Cao).

rely on the development of carbon-based materials and on the continued supply of energy. This energy is either in the form of gasoline or electricity, and is generated mainly from fossil fuels such as coal and oil.

Over the past several decades, significant progress has been made in developing alternative technologies to harvest and use clean, sustainable energy including solar energy, wind power, biofuels, and hydrogen, as well as clean energy technologies, such as fuel cells and lithium-ion batteries. Although these types of energy sources have played a marginal role in the past, new technology is progressing impressively to make alternative energy more practical and often price competitive with fossil fuels. It is expected that the coming decades will usher in a long expected transition away from coal and oil as our primary fuel.

Carbon materials have been playing a significant role in the development of alternative clean and sustainable energy technologies. For example, fullerene-containing *p*-type semiconducting polymers are one of the key foundations in rapidly advancing organic photovoltaics [1-4]. Additionally, carbon nanotubes and graphenes are emerging as classes of new carbon materials, and have been investigated as critical additives for the next generation of optically transparent electronically conductive films for solar cells [5-7]. Carbon nanotubes and graphenes are also studied for the development of batteries, supercapacitors, and fuel cells [8-15].

Carbon assumes an array of structural forms, such as diamond, graphite, graphene, fullerenes, carbon nanotubes, and amorphous carbon [16,17]. The latter can be further divided into soft carbon (carbon that can be easily graphitized), hard carbon (carbon that cannot be easily graphitized), or diamond-like carbon and graphitic carbon, depending on where these materials are used. The diamond-like carbon has  $sp^3$  hybridization, while graphitic carbon has  $sp^2$  hybridization. Both diamond and diamond-like carbon possess excellent mechanical properties, optical properties, and thermal conductivity. This is largely due to the small size and close packing of carbon atoms, as well as short and strong chemical bonds between these atoms. Graphite and graphitic carbons, on the other hand, are excellent electrical conductors. Graphene, carbon nanotubes, and fullerenes are all derivatives of graphite and have attracted significant attention lately in the research community, partly due to their unique and technically important physical properties.

Highly porous carbon has been widely used as catalyst supports, filters, sorbents, scaffolds, and matrices in many technically important fields. Examples include water purification [18-20], artificial livers or kidneys [21-24], and catalyst support [25-28], among others. Highly porous carbon can be divided into two groups: (1) derived from naturally occurring carbonaceous precursors such as coal, wood, coconut shells, fruit stones, and other agricultural byproducts [29-33] and (2) synthetic porous carbon [34-36]. There are a number of ways to synthesize porous carbon, examples of which include sol-gel processing [37-39], etching of metal carbides [40-42], and templated carbon [43-46].

This review article summarizes the recent research progress on the synthetic porous carbon for energy storage and conversion applications: (a) electrodes for supercapacitors, (b) electrodes in lithium-ion batteries, (c) porous media for methane gas storage, (d) coherent nanocomposites for hydrogen storage, (e) electrocatalysts for fuel cells,

(f) mesoporous carbon (MC) for lithium-sulfur batteries, and (g) porous carbon for lithium-oxygen batteries.

## Highly porous carbon for supercapacitors

The most efficient hybrid vehicles lack power and the models that accelerate quickly do so with the assistance of large internal combustion engines. This significantly degrades their fuel efficiency, barely making the extra cost worthwhile in terms of fuel efficiency [47]. While batteries in these vehicles are capable of storing large quantities of energy, they cannot be charged or discharged quickly. This lack of power density requires the battery packs to be oversized, resulting in increased vehicle weight and reduced efficiency. As with the poor discharge rate, battery charging is limited by the same kinetics, thus reducing efficiency gains through full regenerative braking. Additionally, the peak power demands that are placed on the battery packs degrade the life of the battery, reducing the overall longevity of the vehicle [48]. An ideal electrical energy storage device will have high cycle life as well as high energy and power density when measured in terms of weight, volume, and cost.

According to the charge storage mechanism, there are two types of electrochemical capacitors (ECs). One is the electrochemical double layer capacitors (EDLCs) based on activated carbons with capacitance proportional to the electrode surface area (the related mechanism illustration in Fig. 1b). The other, known as pseudo-capacitors or redox supercapacitors, uses transition metal oxides or electrical conducting polymers as electrode materials, with the charge storage depending on the fast *Faradaic* redox reactions. As for the EDLCs, the capacitance at one electrode interface is given by  $C = \epsilon A / 4\pi t$  (where  $\epsilon$  is the dielectric constant of the electrical double-layer region,  $A$  the surface-area of the electrode, and  $t$  the thickness of the electrical double layer). Obviously, the combination of high surface area and small charge separation is necessary for an extremely high capacitance.

EDLCs, also known as supercapacitors, operate by adsorbing/desorbing charged ions from an electrolyte onto their highly porous high surface area electrodes. While traditional capacitors rely on a dielectric material to store a charge, EDLCs rely on the charge of the adsorbed double layer. The capacitance of traditional dielectric capacitors is limited by the thickness of the dielectric material, which separates the charge. The thinnest dielectric materials are 2-5  $\mu\text{m}$  in thickness [49]. However, in the case of EDLCs, charging is achieved by dissociation of ions in the electrolyte salts, resulting in charge separation distances on the order of 1 nm. This arrangement occurs inside the pores of high surface area carbon materials. When the electrode is biased, a double layer structure is developed with the opposite charge accumulated near the electrode surface. The double layer thickness is related to the Debye screening length in the modified Gouy-Chapman model. The double layer capacitance ( $C$ ) is related to the surface area, the effective dielectric constant ( $\epsilon$ ), and the double layer thickness ( $d$ ) by an inverse linear relationship ( $C = \epsilon A / d$ ). A typical smooth surface will have a double layer capacitance of about 10-20  $\mu\text{F}/\text{cm}^2$ , but if a high surface area electrode

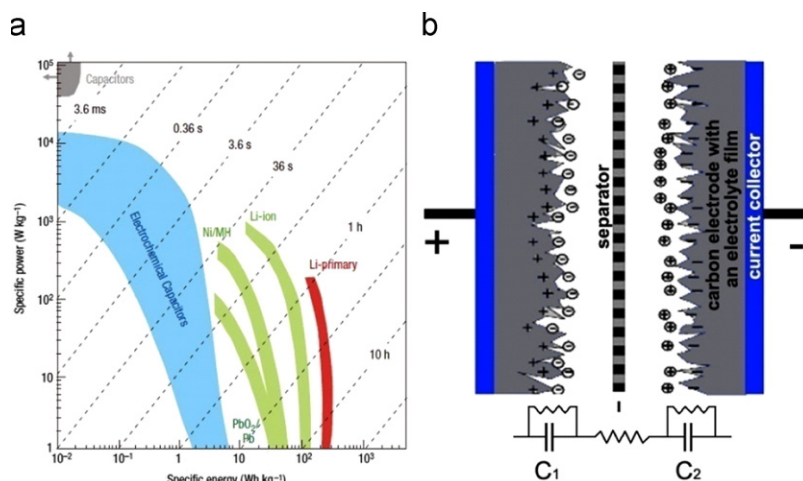


**Figure 1** (a) Specific power against specific energy for various electrical energy storage devices [54]. (b) Illustration of an electrochemical double layer capacitor with simplified electric circuit.

surface is used, the capacitance can be increased to 100 F/g for conducting materials that have a specific surface area of 1000 m<sup>2</sup>/g [50]. A wide range of high surface area carbon materials have been investigated, including activated carbon and multi- and single-walled carbon nanotubes. The capacitance typically ranges from 40 to 140 F/g for activated carbon [51] and from 15 to 135 F/g for carbon nanotubes [52,53]. Currently, the best available result from commercial products is about 130 F/g from Maxwell's Boost-Cap. Compared with other electrical energy storage devices (Fig. 1), ECs can be fully charged or discharged in seconds. Although their energy density (~5 Wh/kg) is lower than that of batteries, they have high power density (10 kW/kg) about 10 times larger than in secondary batteries [54,55].

### High surface area carbon for supercapacitors

Current EDLCs in the market are produced by pyrolyzing and activating wood, plant matter, petroleum sources, and phenolic resins (including aerogels and cryogels), among others [56,57]. Naturally derived electrodes contain great amounts of impurities or ash, which can compromise the EDLC performance [58] due to unwanted *Faradaic* reactions that can degrade the electrolyte. In addition, the pore size is limited by what nature provides and may vary from source to source. Sol-gel derived carbon cryogels and carbon aerogels, on the other hand, have good conductivity, high surface area, controlled bulk and surface chemistry, and tunable porous structure, rendering them excellent candidates as electrodes for supercapacitors with high energy density and long cyclic stability [59-62]. Carbon nanotubes and graphenes have also been used in the manufacturing of batteries and supercapacitors because of their high conductivity [57,63].

Carbon materials based supercapacitors have been the subject of several excellent reviews [51]. There are several approaches to improve charge storage in carbon supercapacitors. A higher capacitance can be achieved by careful thermal, chemical, or electrochemical treatment to increase the accessible surface area and surface functional groups, or by extending the operating voltage range beyond

the limit of an aqueous electrolyte solution. Several critical factors contribute to a high capacitance. First, increasing the surface area is quite important, but significant effort has already been made to maximize the surface area of carbon. The room for further improvement from pure surface area is limited. For many high surface area materials, the correlation between the surface area and the specific capacitance cannot be strictly established. Second, inducing pseudocapacitance can increase the capacitance. This involves voltage dependent *Faradaic* reactions between the electrode and the electrolyte, either in the form of surface adsorption/desorption of ions, redox reactions with the electrolyte, or doping/undoping of the electrode materials. Surface functionalization proves to be effective in increasing the pseudocapacitance arising from oxidation/reduction of surface quindoidal functional groups generated during the sample treatment [64,65].

Another widely investigated method to enhance the performance is to coat the carbon materials with conducting polymers such as polyaniline and polypyrrole or redox active metal oxides such as manganese oxides [66-68]. For example, polypyrrole coated carbon nanotubes can attain a capacitance of 170 F/g [69]. While doped conducting polymers can have high capacitance, the stability of the organic materials has so far limited their applications. The best example of redox pseudocapacitance is hydrous RuO<sub>2</sub>, which shows a continuous redox activity over a wide voltage range and very high capacitance, independent of surface area. However, RuO<sub>2</sub> is very expensive due to limited supply. Much work has been focused on replacing RuO<sub>2</sub> with other metal oxides and nitrides. For example, the self-limiting reaction of aqueous permanganate (MnO<sub>4</sub><sup>-</sup>) with carbon nanofoams produces conformal, nanoscopic deposits of birnessite ribbons and amorphous MnO<sub>2</sub> throughout the ultraporous carbon structure. The MnO<sub>2</sub> coating contributes additional capacitance to the carbon nanofoam while maintaining the favorable high-rate electrochemical performance inherent to the ultraporous carbon structure of the nanofoam. Such a three-dimensional design exploits the benefits of a nanoscopic MnO<sub>2</sub>-carbon interface to produce an exceptionally high area-normalized capacitance (1.5 F/cm<sup>2</sup>), as well as high volumetric capacitance (90 F/cm<sup>3</sup>) [70].

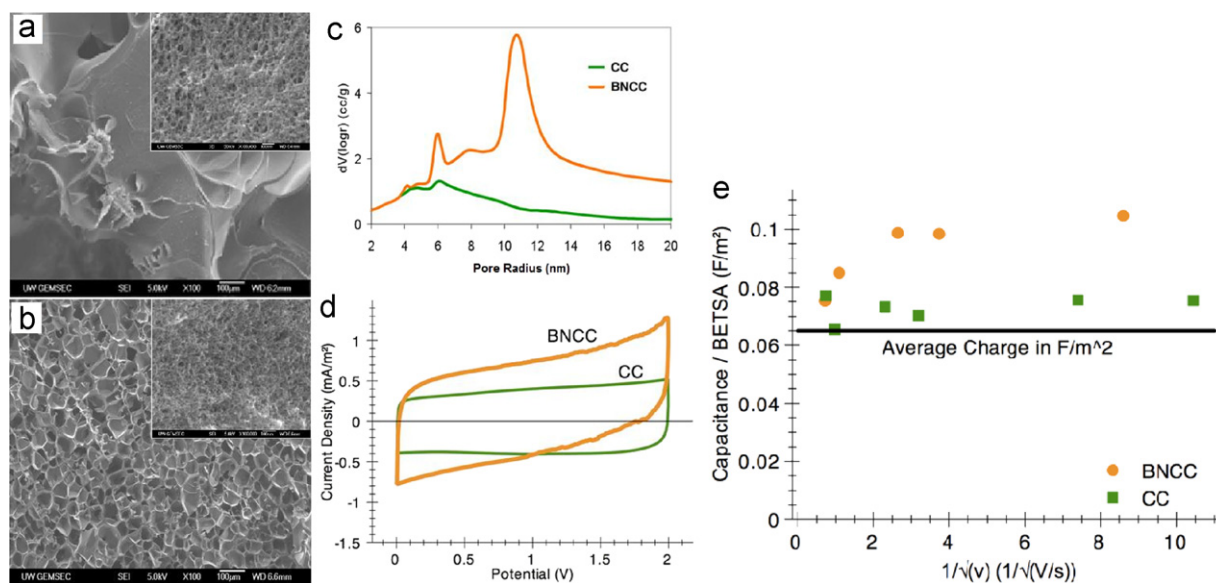


**Figure 2** (a)-(d) Microstructure effect of chemically treated carbon cryogels. SEM images of (a) CC and (b) BNCC with high magnification images inserted in top right corners. Comparison of (c) pore size distribution and (d) C-V curves of CC and BNCC samples. (e) Capacitance of samples vs.  $1/\sqrt{v}$ . The constant behavior of CC is characteristic of mesopores or larger pore structures that are not affected by the electrolyte penetration [77]. On the other hand, pseudocapacitance increases the charge storage capabilities of carbon in the BNCC sample [74].

Additionally,  $\text{MnO}_2$  coated carbon nanotubes can attain a capacitance of 140 F/g [71-73], but like conducting polymers, these composite materials still do not resolve the fundamental limitations of  $\text{MnO}_2$ , with limited stability and operating voltage range.

Chemical modification of carbon cryogels is used as an efficient approach for altering both their porous structure and surface chemistry, which has been shown to result in much improved electrochemical properties (Fig. 2) [74]. The experiments involve the transportation of ammonia borane ( $\text{NH}_3\text{BH}_3$ ), dissolved in anhydrous THF solvent, to the pores of resorcinol-formaldehyde hydrogels during post-gelation solvent exchange. After being soaked in the  $\text{NH}_3\text{BH}_3$  solution, the modified hydrogels underwent the same freeze-drying and pyrolysis processes as unmodified hydrogels. The resultant modified carbon cryogels are referred to as BNCC, indicating the samples were being boron and nitrogen co-doped, whereas the unmodified carbon cryogels are referred to as CC samples. Fig. 2a and b compares the typical SEM images of CC (a) and BNCC (b) samples. The inserts on the top-right corners are the high-magnification SEM images, revealing the highly nanoporous nature in both samples; however, the relatively low-magnification SEM images differ greatly. From the SEM images, it is evident that the BNCC sample possesses a rather uniform macroporous structure, whereas the CC sample possesses negligible macroporous features under low magnification. Such a difference in porous structure is verified by the pore size distributions derived from the nitrogen sorption isotherms, as shown in Fig. 2c. It is evident that BNCC possesses much larger pores ( $>5$  nm), which results in an increase in pore volume, meanwhile maintaining a similar number of smaller pores ( $<5$  nm) as CC samples. Also included in Fig. 2d are the C-V curves of BNCC and CC samples, indicating improved electrochemical properties when the carbon cryogels are co-

doped with boron and nitrogen. Fig. 2e compares the capacitances per unit specific surface area as a function of reciprocal square-root of voltage rate,  $1/\sqrt{v}$ , for the BNCC and CC samples. The carbon co-doped with B and N possessed 30% higher specific capacitance than that of the CC at higher frequencies. This increase in the specific capacitance is Faradaic in nature, either from the dopants or  $\text{B}_2\text{O}_3$ . This improved capacitive behavior has been observed in these carbon materials due to the presence of active species, which contribute to the total specific capacitance by the pseudocapacitive effect. At the same time, large specific surface area and porosity are also essential for high current density and charge storage [58,75,76]. These improvements in electrical and electrochemical properties are expected to significantly enhance the efficient energy storage in both supercapacitors and hybrid batteries.

A new family of porous carbon called carbide-derived carbon (CDC) has been developed recently through selective removal of non-carbon atoms from carbides upon high-temperature treatment (e.g., chlorination) [40,79]. The porous structure, including average pore size, pore size distribution, pore volume, and specific surface area of CDC can be tailored through selection of the precursor (e.g., composition and structure of carbides) and the chlorination conditions. CDC with specific surface area  $>3100$   $\text{m}^2/\text{g}$  and pores of  $\sim 0.3$ -10 nm [80] makes a promising material supercapacitor electrode [41,78,81].

Most recently, Presser et al. [82] reported nano-fibrous felts (nano-felts) of carbide-derived carbon developed from electrospun titanium carbide (TiC) nanofelts as the precursor. Conformal transformation of TiC into CDC conserves the main features of the precursor, including the high interconnectivity and structural integrity; the developed TiC-CDC nano-felts are mechanically flexible/resilient, and can be used as an electrode material for supercapacitor

applications without the addition of any binder. After synthesis through chlorination of the precursor at 600 °C, the TiC-CDC nano-felts show an average pore size of  $\sim 1$  nm and a high specific surface area of 1390 m<sup>2</sup>/g, and the nano-fibers have graphitic carbon ribbons embedded in a highly disordered carbon matrix. Graphitic carbon is preserved from the precursor nano-fibers where a few graphene layers surround TiC nanocrystallites. Electrochemical measurements show a high gravimetric capacitance of 110 F/g in aqueous electrolyte and 65 F/g in organic electrolyte. Because of the unique microstructure of TiC-CDC nano-felts, a reduction in the capacitance of merely 50% at a high scan rate of 5 V/s is observed. A reduction of just 15% is observed for nano-felt film electrodes tested in 1 M H<sub>2</sub>SO<sub>4</sub> at 1 V/s, resulting in a high gravimetric capacitance of 94 F/g. Such a high rate performance is known only for graphene or carbon-ion based supercapacitors, in which binders have to be used for the fabrication of those supercapacitors.

Interconnected mesoscale porosity plays an important role in ensuring that charged ions can freely access all the surfaces (2-50 nm). As a result, many groups investigated surfactant templated mesoporous carbon that has controllable pore sizes [83,84]. However, recently, a new study reported the effect of pore sizes on the charge storage properties and provided new information on the relative role of the mesoscale and microscale porosity (Fig. 3) [78]. In Fig. 3a, the charge storage in carbide derived carbon by high temperature chlorination is reported. This material has precise control of the pore sizes down to less than 1 nm. Three regions are observed. In Region I where the mesopore dominates, the capacitance increases with the pore sizes due to better pore accessibility and less overlapping of the double layer structure. However, as the pore size becomes smaller in Region II, the capacitance begins to increase. In Region III, the capacitance increases sharply with decreasing pore sizes. The effect of the ultra-small pore on the capacitance is attributed to the distortion of the double layers in the small pores and decrease in the double layer thickness.

## Carbon nanotubes (CNTs) for supercapacitors

CNTs with large surface areas have been extensively studied in supercapacitors, with specific capacitances of 4-180 F/g in a solution of H<sub>2</sub>SO<sub>4</sub> or KOH [53,64,85-88], and may have advantages over traditional carbon (Fig. 4). The specific surface area and the pore size of the CNTs remarkably affect the capacitance [89]. For example, Niu et al. prepared MWNT ECs with specific surface area of  $\sim 430$  m<sup>2</sup>/g, showing a specific capacitance of 113 F/g using a solution of 38 wt% H<sub>2</sub>SO<sub>4</sub> as the electrolyte [85]. An et al. obtained a maximum specific capacitance of 180 F/g with a large power density of 20 kW/kg by heating CNTs to enhance their specific surface and pore distribution [88]. However, the specific surface area of CNTs is unsatisfying for excellent ECs compared with other activated carbon electrodes (specific surface area up to 3000 m<sup>2</sup>/g) or mesoporous carbons (up to 1730 m<sup>2</sup>/g) [90,91]. Researchers also tried to treat the surfaces of CNTs with ammonia, aqueous NaOH/KOH solution, or nitric acid to introduce oxygen functional groups (carboxyl, phenolic, lactone, aldehyde, ether groups, etc.), and thus improve the electrochemical properties of the electrodes [92-94]. Yoon et al. increased the capacitance of the CNT electrode from 38.7 to 207.3 F/g through surface treatment using ammonia plasma [92]. However, some scientists think that the oxygen groups will lead to capacitor instability with an increased resistance and deterioration of capacitance [95,96]. In addition, the introduction of surface oxygen groups to the CNT electrode would not work with organic electrolyte.

The specific power of supercapacitors is  $P_{max} = V^2/4R$ , where  $V$  is the working voltage and  $R$  the equivalent series resistance. The resistance is comprised of the electronic resistance of the electrode material, the interfacial resistance between the electrode and the current-collector, the diffusion resistance of ions moving in small pores of the electrode material, or other resistances [95,98]. That is, the characteristics of the electrode materials and the type of fabricated electrode become the key

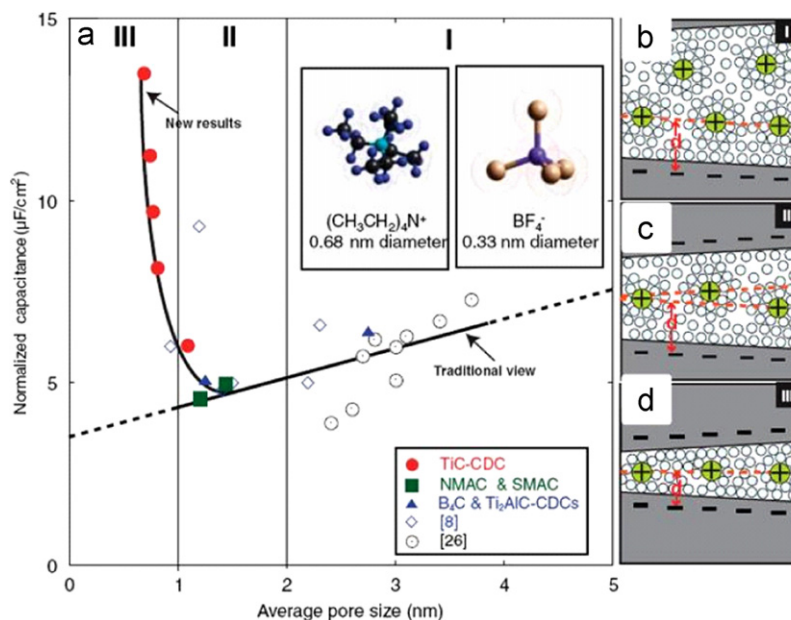


**Figure 3** Effect of pore sizes on charge storage in carbide derived carbon materials [78]. (a) Normalized capacity as a function of pore sizes. (b)-(d) Ion transport in different pore regimes.

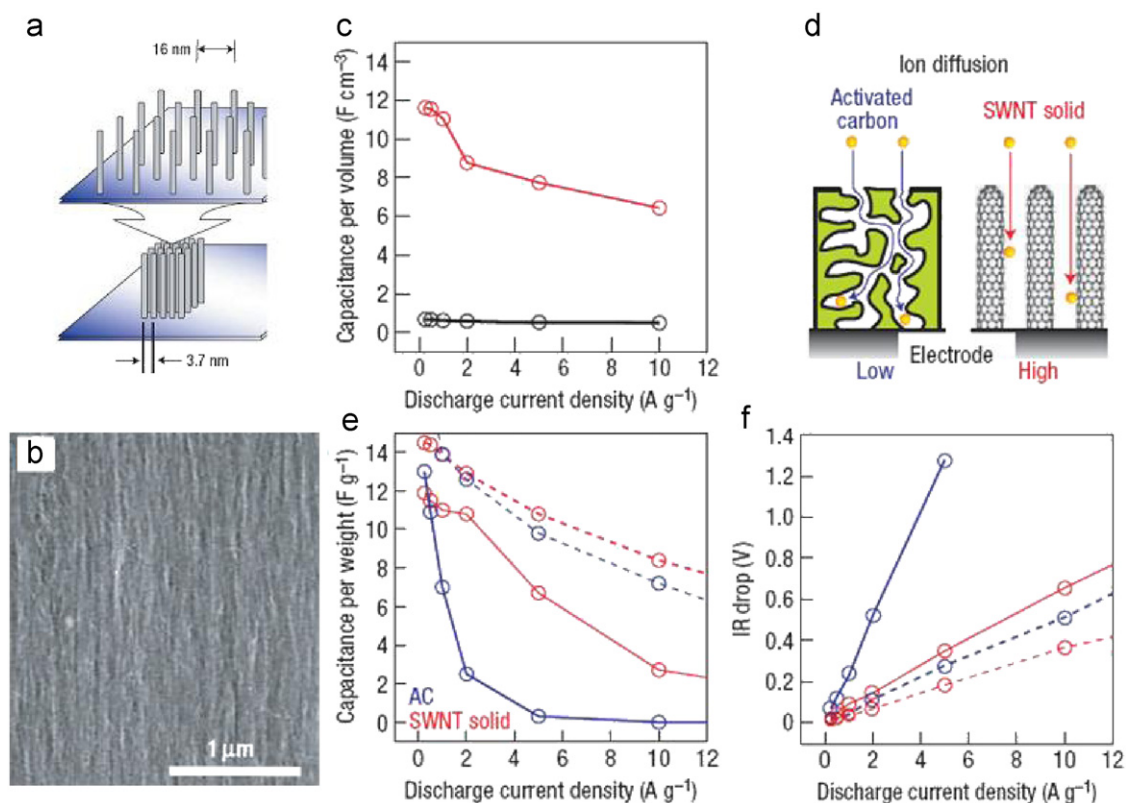


**Figure 4** Comparison of activated carbon and oriented carbon nanotubes. (a) Fluid drying to form dense solid carbon from long single wall carbon nanotubes (SWCNTs). (b) TEM image of the nanotube solid. (c) Capacitance per volume for dried (red) and as prepared (black) SWCNTs. (d) Ion diffusion in activated carbon and oriented CNTs. (e) Specific capacitance as a function of current density. Results from CNTs are in red, and activated carbon is in blue. (f) Potential drop as a function of current density [97].

factors for excellent performance, such as the density of CNT arrays [99]. There are several routes to enhance the supercapacitors' energy storage properties:

- (1) Growing or depositing CNTs directly on the current collector (Ni, Al, alloy, or other metals) as electrodes, reducing the contact resistance [85,88,92,100-102]. Forming this binder-free CNT film electrode would enhance its electrochemical performance as it has less impurities introduced by the polymer binders. Some groups even designed lightweight electrodes using dense CNT networks as both the current collector and the active electrode material for ECs [103].
- (2) Combining CNTs with transition metal oxides (RuO<sub>2</sub>, NiO, MnO<sub>2</sub>, In<sub>2</sub>O<sub>3</sub>, etc.) or conducting polymers such as polyaniline (PANI), polypyrrole (Ppy), or other polymers [106-111]. The hybrid composites are promising since they can combine two hybrid materials together to gain the largest capacitance by dual storage mechanisms (EDLC and pseudocapacitance) [112]. In a hybrid system, conducting polymers or some metal oxides have a very large specific capacitance (e.g. 775 F/g for PANI, 480 F/g for PPy, theoretical value of MnO<sub>2</sub> ~1100 F/g) [113-115], contributing to the overall capacitance, while CNTs play the role of a perfect backbone and a good conductor for the composite during long cycling. Typical results from a hybrid composite electrode are shown in Fig. 5a. Au-segmented MnO<sub>2</sub>/CNTs hybrid coaxial electrodes were

fabricated for high-power supercapacitors [104]. The CNTs improve electronic conductivity and the Au tips between the MnO<sub>2</sub>/CNTs arrays and the collector lower the contact resistance. Interestingly, the designed CNTs-based composite supercapacitor device (in Fig. 5b), with room temperature ionic liquid (RTIL) as an additive, increases the operating temperature range (195-423 K, commercially available at 233-358 K) [105].

- (3) Integrating both the advantages of ECs and Li-ion batteries to fabricate a new hybrid EC. For example, the Li group developed the hybrid EC, using the synergistic effects of a CNT cathode and a TiO<sub>2</sub>-B nanowire anode, showing an energy density of 12.5 Wh/kg, which is twice as high as a CNT-CNT supercapacitor (6.1 Wh/kg) [116].

## Graphene based supercapacitors

Graphene-based supercapacitors are attracting a lot of research attention and demonstrated a specific capacitance a little over 100 F/g [117-119]. It is necessary to modify or dope graphene to enhance its electrochemical properties. One way is to prevent single or few layered graphene sheets from agglomeration, so as to obtain higher effective surface area. Wang et al. used a gas-solid reduction process to avoid aggregation and achieved a maximum specific capacitance of 205 F/g at 1.0 V in aqueous electrolyte with an energy density of 28.5 Wh/kg [120], which is better than CNT-based

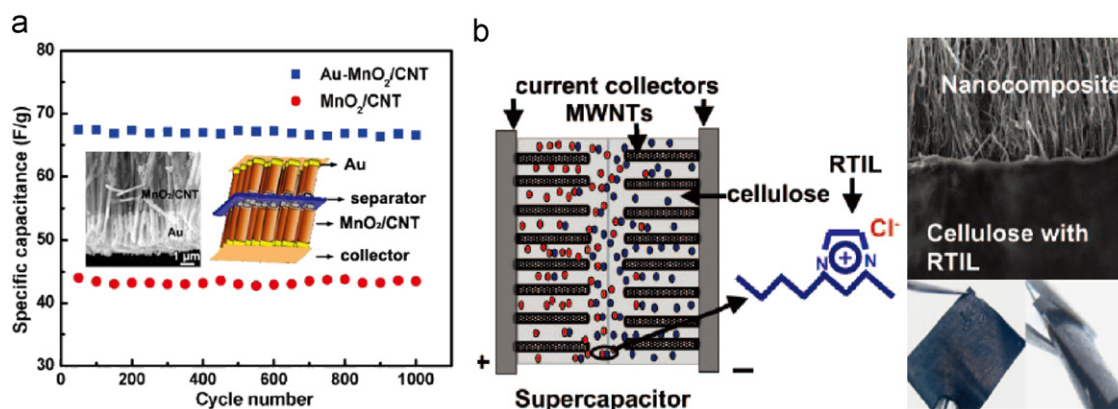


**Figure 5** (a) Specific capacitance plots show the stable EC with Au-MnO<sub>2</sub>/CNT electrodes (the inset shows its fabrication and the related SEM image) is better than that with MnO<sub>2</sub>/CNT electrode [104]. (b) Fabrication of nanocomposite EC (the corresponding SEM image is shown on the right) with additive RTIL. The right bottom picture reveals the flexibility of the composite paper [105].

supercapacitors [53,64,85-88]. Liu et al. fabricated supercapacitors with curved graphene and obtained the highest energy density (85.6 Wh/kg at 1 A/g at room temperature or 136 Wh/kg at 80 °C) reported so far [121].

Another way to enhance the storage capacity is to combine graphene with other nanomaterials and fabricate hybrid composite electrodes [122-133]. Various hybrid composites were synthesized, such as graphene (or grapheme oxide)-polyaniline composites [122-126], graphene nanosheet-CNTs-PANI composites [127], graphene-CNTs composites [128], graphene-metal oxide composites [129,130,134], graphene-metal hydroxide composites [131,132], and graphene-Sn<sub>3</sub>S<sub>4</sub> composites [133]. For example, the composite electrode of PANI nanowire arrays aligned vertically on graphene oxide nanosheets showed a synergistic effect of PANI and graphene oxide, with higher electrochemical capacitance and better stability than each individual component [122].

Graphene nanosheets have also awakened research interests in other fields, such as photocatalysis [135], direct methanol fuel cells [136], electrochemical cells [137], electrochemical biosensing [138-142], and even providing platforms for sensing TNT [143], studying charge transport [144], and analyzing small molecules by matrix-assisted laser desorption/ionization time-of-flight mass spectrometry [145].

## Li-ion batteries

### Graphite and high surface area carbon

Lithium-ion batteries have replaced a great deal of older battery systems, such as nickel metal hydride, particularly in high-tech devices like laptops and cell phones. This is mainly due to their high energy density and long cycle life [146-148]. However, lithium-ion batteries still cannot satisfy the needs for high specific power and energy storage applications, such as power tools, electric vehicles, and efficient use of renewable energies [149].

Carbon plays a particularly important role in the development of Li-ion batteries. Prior to the discovery of graphite anode materials, Li metal had been the main candidate for Li-ion batteries, but it had a serious problem of dendrite

formation, which caused a short circuit and presented a safety issue. The use of graphite in rechargeable batteries has been proposed a long time ago [150] and later as the anode material for intercalating Li ions [151]. Till date graphite is still the main anode material for commercial Li-ion batteries and the topic has been extensively reviewed in the literature [152]. Graphite is attractive because of its high in-plane electron conductivity due to the  $\pi$ -bond and weak interaction with Li ions, giving rise to high Li ion storage capacity and fast Li ion diffusion (Fig. 6a).

Unfortunately, the intercalation capacity of Li ions in graphite is still limited (372 mAh/g, LiC<sub>6</sub>). Great efforts have been made to increase this capacity by altering the carbon structures, increasing lattice disordering, creating pore spaces, and increasing surfaces areas. The excessive Li ion storage capacity could be derived from excessive bulk storage due to the formation of different species, such as the proposed formation of Li<sub>2</sub> molecules in polymer derived carbon with a large interlayer spacing of 0.4 nm. The excessive capacity could also result from storage in microcavities or nanopores (Fig. 6b) [153]. Another important mechanism is Li storage on the surfaces and interfaces of microcrystalline or nanocrystalline graphite or stacked graphene sheets (the house-of-cards model) (Fig. 6c) [154-157]. On the surfaces and interfaces the Li storage capacity can be much larger than 372 mAh/g. The key to achieving the high capacity is to control the starting materials and the processing conditions (temperature for example).

### CNTs for Li-ion batteries

As one kind of porous carbon materials, carbon nanotubes (CNTs) have been extensively investigated as anode materials for Li-ion batteries due to their mesoporous character (higher electrode/electrolyte contact area leading to higher charge/discharge rates), high chemical stability, low resistance (short path lengths for electronic and Li<sup>+</sup> transport), strong mechanical strength, and high activated surfaces (better accommodation of the strain of Li<sup>+</sup> insertion/removal, improving cycle life) [158-161].

In comparison to the theoretical maximum capacity of graphite at 372 mAh g<sup>-1</sup> (LiC), the electrochemical

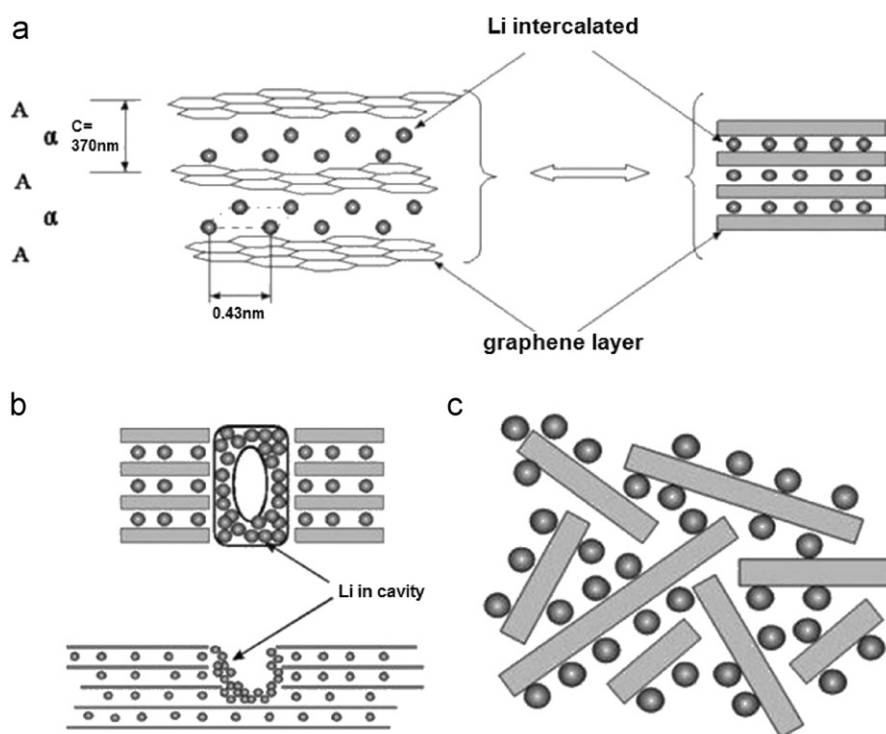


**Figure 6** Li ion storage mechanisms in graphite [152]. (a) Li ion intercalation in graphite. (b) Li ion storage in micro- or nanocavities. (c) Li ion storage on surfaces or at the interfaces of graphite micro- or nanocrystals (house-of-cards model).

intercalation of lithium in multi-wall and single-wall carbon nanotubes (MWNs, SWNTs) and typically synthesized SWNTs (Fig. 7) have been studied with higher capacities in recent years [158-166]. MWNs exhibited reversible capacities of 80-640  $\text{mAh g}^{-1}$  ( $\text{Li}_{0.2}\text{C}_6$ - $\text{Li}_{1.7}\text{C}_6$ ), while the capacity of the SWNTs was 450-600  $\text{mAh g}^{-1}$  ( $\text{Li}_{1.2}\text{C}_6$ - $\text{Li}_{1.6}\text{C}_6$ ), which could increase to 790 and 1000  $\text{mAh g}^{-1}$  ( $\text{Li}_{2.1}\text{C}_6$  and  $\text{Li}_{2.7}\text{C}_6$ ) by either mechanical ballmilling or chemical etching [159-166]. However, the nature of carbon materials restricts their capacity, although some scientists fabricate particular microstructures to improve the electrochemical properties of CNTs. For example, 1D highly aligned CNT arrays were prepared by the chemical-vapor-deposition (CVD) method [167,168]. Noticeably, the Fisher group fabricated a tube-in-tube structure (CNTs  $\sim 20$  nm in diameter within the template-synthesized CNTs  $\sim 250$  nm in diameter, Fig. 7a) with  $\text{Li}^+$  intercalation capacity two times higher than that of the template-synthesized CNTs, as the inner tubules provided more electrochemical active sites for intercalation of Li ions [169].

Obviously, the most direct way to improve the capacity of the CNT anodes is to fabricate composite electrodes of CNTs with other materials. In such hybrid systems, the CNTs function as an effective confining buffer of mechanical stress induced by volume changes in charging and discharging reactions, while the other nanomaterials provide a high capacity. By developing different systems such as metal (Sn, Sb, Bi, etc.)-C, metal oxide ( $\text{SnO}$ ,  $\text{SnO}_2$ ,  $\text{MnO}_2$ ,  $\text{Fe}_2\text{O}_3$ ,  $\text{Fe}_3\text{O}_4$ ,  $\text{CuO}$ , etc.)-C, Si-C, and alloy (SnSb, SnCo, SnMn, SnFe, AgFeSn, etc.)-C, many researchers have demonstrated that these electrodes showed high charge capacities and good durability [136,170-184]. For example, the reversible capacities of CNT-56 wt %  $\text{SnSb}_{0.5}$  composites were as high as 518  $\text{mAh g}^{-1}$  with a decreasing rate of only 1.1% per cycle

within 30 cycles [170]. The Si-C nanocomposites have attracted considerable attention because of their specific capacity as high as 4200  $\text{mAh g}^{-1}$  ( $\text{Li}_{22}\text{Si}_5$ ), the maximum Li-containing alloy phase in the Li-Si system. It was demonstrated that the hybrid Si-CNTs exhibited high reversible capacity of  $\sim 2000$   $\text{mAh g}^{-1}$  with a very little fade in capacity of  $\sim 0.15\%$  per cycle over 25 cycles [171].

Even in the composite anode nanomaterials based on CNTs, the microstructure is still the focus for high-performance Li-ion batteries. For example, Reddy et al. synthesized tubular coaxial  $\text{MnO}_2$ /CNT array electrodes with a unique combination of high porosity and low internal resistance (Fig. 7c) [185]. The Li group fabricated coaxial CNTs/ $\text{MoS}_2$  nanomaterials; electrochemical measurements revealed that the  $\text{MoS}_2$  sheath improved the lithium storage/release properties at the nanoscale through a unique synergy [187]. Smarter, smaller, lighter, and greater energy density would be the demands for portable battery technology in the near future. The flexibility, porosity, and conductivity of CNT membranes gave scientists an insight on fabricating "paper electrodes" [186,188-190]. SWNTs were used to fabricate free-standing electrode without polymer binder or a metal substrate, but the capacity was unsatisfactory [187]. CNT networks and aligned CNTs/conducting polymer were then exploited for paper electrodes, and the capacity of the latter was 50% higher than that of SWNT paper electrode [189,190]. In particular, the Cui group developed CNTs/Si film free-standing electrodes with high specific charge storage capacity  $\sim 2000$   $\text{mAh g}^{-1}$  and good cycling performance (Fig. 7d) [186]. Later, vertically aligned Si/CNT arrays prepared by the Kumta group also had a capacity of 2000  $\text{mAh g}^{-1}$  [191]. Hybrid paper electrodes exhibit a promising research prospect.

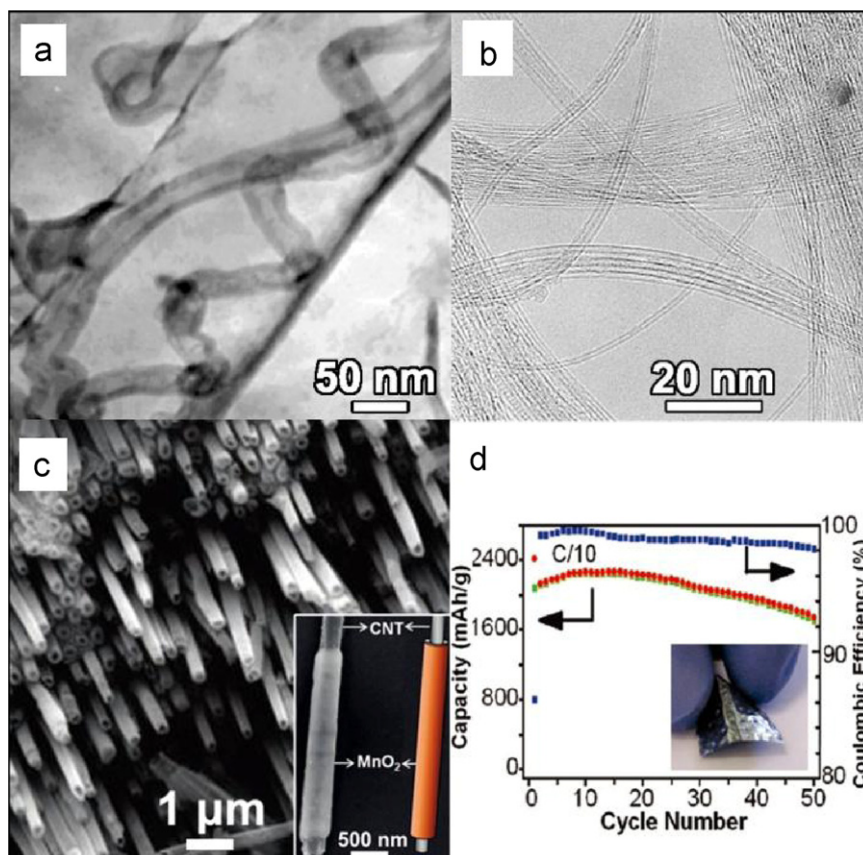


**Figure 7** CNTs with various morphologies as anode materials: (a) CNTs with tube-in-tube structure [169]; (b) ultrathin SMNTs [159]; (c) coaxial  $\text{MnO}_2/\text{CNT}$  array [185]. (d) Charge, discharge and Coulombic efficiency versus cycle number for a half cell using free-standing CNT-Si films as the working electrode [186].

In summary, CNTs as one kind of classical porous carbon materials with a mature studied history will play a significant role in the battery market of the near future, but how to combine hybrid materials together to obtain safe, stable, and high-capacity electrodes has always been the radical problem that many researchers are trying to solve.

### Graphene (including graphene oxide, GO) for Li-ion batteries

Recently, graphene, composed of monolayers of carbon atoms arranged in a honeycombed network, has emerged explosively and attracted much attention in the fields of materials science and condensed-matter physics [192-194]. As the thinnest carbon materials, graphene and graphene-based materials have promising application in energy-related electrochemical devices, such as Li-ion batteries, ECs, fuel cells, and solar cells [195-197]. In particular, these materials have superior electrical conductivities to graphitic carbon, higher surface area of over  $2600 \text{ m}^2/\text{g}$  than CNTs, and a broad electrochemical window that would be more advantageous in energy storage. Thus, a series of research work on Li-ion batteries and ECs based on graphene or graphene oxide were performed intensively with the similar routes to the CNTs-based electrode materials for Li-ion batteries.

Some scientists used graphene sheets directly as an anode material for lithium-ion batteries and found that they had improved electrochemical properties. For example, the first reversible specific capacity of the prepared graphene sheets with specific surface area of  $492.5 \text{ m}^2/\text{g}$  was as high as  $1264 \text{ mAh g}^{-1}$  at a current density of  $100 \text{ mA/g}$ . After 40 cycles, the reversible capacity was still kept at  $848 \text{ mAh g}^{-1}$  at the current density of  $100 \text{ mA/g}$ , higher than general values of CNT electrodes [198]. Although graphene nanostructures were thought to have significant disorder and defects, which might lower their electrical conductivity, some reports verified highly disordered graphene nano-sheets as electrodes with high reversible capacities ( $794\text{--}1054 \text{ mAh g}^{-1}$ ) and good cyclic stability [199]. The surface oxidation of carbon materials could improve their electrochemical properties [200], and Bhardwaj et al. confirmed that oxidized graphene nanoribbons (ox-GNRs) outperformed MWNTs and GNRs, presenting a first charge capacity of  $\sim 1400 \text{ mAh g}^{-1}$  and a reversible capacity of  $\sim 800 \text{ mAh g}^{-1}$  [201].

However, the increase was not satisfying for application in energy technologies. As described in CNT-based electrodes, an efficient way to improve the Li-ion insertion properties is to introduce hybrid nanostructured electrodes that interconnect nanostructured electrode materials with conductive additive nanophases. Regarding the graphene (graphene oxide)-based electrode materials, various hybrid nanocomposites have been synthesized, such as the nanocomposites

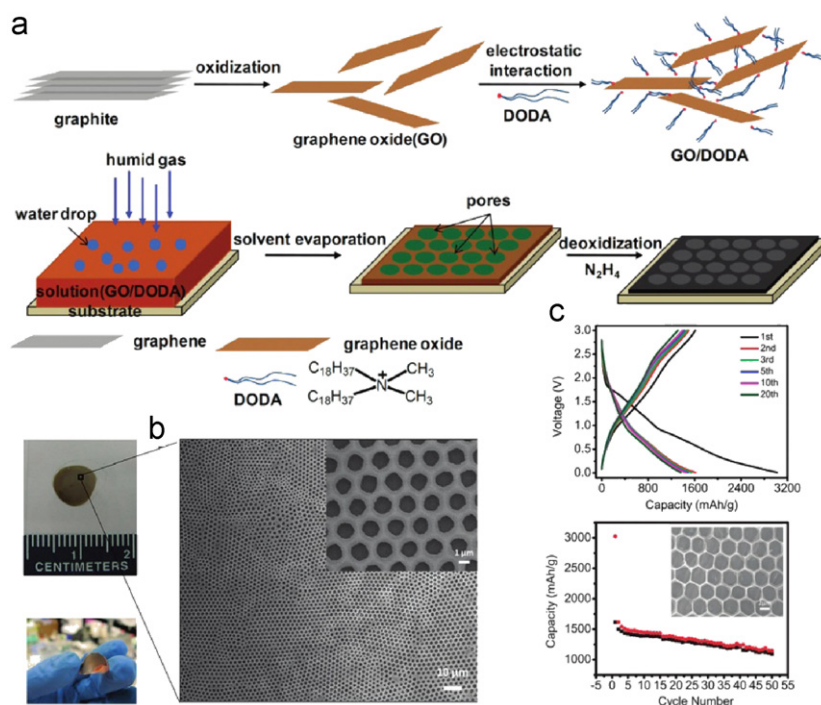


**Figure 8** (a) Illustration for the preparation of the honeycomb structured film based on graphene oxide. (b) SEM images and photograph for the honeycomb structures. (c) Charge and discharge cycle curves of the honeycomb-patterned film as anodes in Li-ion battery at a current density of 50 mA/g (top), capacity versus cycle number for the honeycomb film (bottom) [202].

of metal oxide ( $\text{TiO}_2$ ,  $\text{CuO}$ ,  $\text{CeO}_2$ ,  $\text{SnO}_2$ ,  $\text{Mn}_3\text{O}_4$ ,  $\text{Fe}_3\text{O}_4$ ,  $\text{Fe}_2\text{O}_3$ ,  $\text{Co}_3\text{O}_4$ , etc.) and graphene [203–210], metal hydroxide and graphene [180], nanosized Si and graphene [211], and other hybrid composites [212,213]. In particular, three-dimensional (3D) graphene-based hybrid structures were fabricated to improve the storage capacity of Li-ion batteries by increased specific surface area and more suitable layer spacing of graphene sheets. Some metal oxides, CNTs, fullerenes (C60), carbon nanofibers, and even organic agents could be introduced to fabricate 3D-structured graphene [202,214–216]. For example, Yin et al. created honeycomb-like electrode materials with hierarchical graphene nanoarchitectures modified by the organic agent dimethyldioctadecylammonium (DODA) with electrostatic interaction. This novel structure simultaneously optimized ion transport and capacity, leading to a high performance of reversible capacity (up to  $1600 \text{ mAh g}^{-1}$ ), and  $1150 \text{ mAh g}^{-1}$  after 50 cycles [202] (Fig. 8).

## Hydrogen and gas storage

### Highly porous carbon for hydrogen and methane gas storage

One area of highly porous carbon in energy application that has attracted a lot of attention is as sorbents for hydrogen and methane storage through physisorption [217–222]. Physisorption is a principle where the forces involved are weak intermolecular forces; therefore it is generally associated with fast kinetics and reversibility. But the challenge with the physisorption of hydrogen also results from these weak forces.  $\text{H}_2$  is the smallest molecule and only has two electrons; hence it is hard

to polarize and in the absence of relatively strong polarizing centers, interaction between the adsorbent and the non-polar hydrogen molecules relies on the weak dispersion forces. These are created by temporarily induced dipoles and are typically of the order of 3–6 kJ/mol [223]. Thus, significant hydrogen adsorption often takes place only at a cryogenic temperature. Nanostructured materials may offer advantages for molecular hydrogen storage by providing high surface areas, or by encapsulating or trapping hydrogen in microporous media. Using porous nanostructured materials, in general, can reduce the gravimetric and the volumetric storage densities. Additionally, the increased surface area and porosity in nanostructures will offer additional binding sites on the surface and in the pores that could increase storage mainly through physisorption. The possibility of storing a significant amount of hydrogen on high surface area materials has been a key driver in the investigation of hydrogen sorption properties of nanotubes, graphite sheets, metal organic frameworks, and template ordered porous carbons. Nanostructured carbons, zeolites, metal-organic frameworks, clathrates, and polymers with intrinsic microporosity are examples of the investigated physisorption materials.

Early reports [224,225] on hydrogen storage in carbon nanotubes and graphitic nanofibers proposed high storage capacities (to 67 wt%) and started an extensive worldwide surge of research. Since then many succeeding experiments were carried out with different methods, but such high values have not yet been reproduced by other groups [226]. Furthermore, no hypothesis could support the unusually high storage capacities and, therefore, the high storage capacity results were thought to be more related to the faults of experiment [227,228]. Nevertheless, hydrogen adsorption on carbon materials is still an attractive and improving field.

The result of several investigations proposes that the amount of adsorbed hydrogen is proportional to the specific surface area of the carbon material [229,230]. In the case of activated carbons and activated carbon fibers, the hydrogen absorption of 5 wt% is obtained at low temperature (77 K) and high pressure (30–60 bar) [231]. For graphite nanofibers (GNF), single walled nanotubes (SWNT), and multi-walled nanotubes (MWNT), the reversible hydrogen uptake of 1.5 wt% per 1000 m<sup>2</sup>/g under ambient conditions is reported [232]. Hydrogen capacity of 7 wt% is observed for ordered porous carbon with surface area of 3200 m<sup>2</sup>/g, prepared by template at 77 K and 20 bar [220]. Recent studies on carbon aerogels (CAs), another class of amorphous porous carbon structures with high surface area, show 5 wt% of hydrogen adsorption for surface area of 3200 m<sup>2</sup>/g at 77 K and pressure 20–30 bar (Fig. 9) [233].

Recent research on hydrogen physisorption on carbon nanostructures involves efforts to increase the surface area of carbon to provide more binding sites, and incorporating functional groups (dopants) in carbon to increase the binding energy between hydrogen and carbon surface [234].

In comparison with hydrogen, storage of natural gas receives much less attention, in spite the fact that natural gas is already in relatively widespread use as a transportation fuel [235]. A natural gas powered vehicle produces 70% less carbon monoxide, 87% less NO<sub>x</sub>, and 20% less CO<sub>2</sub> as compared to gasoline powered vehicles [236]. The conventional approaches available today, compressed natural gas (CNG) and liquid natural gas (LNG), have significant drawbacks, including (a) relatively high cost, (b) low storage efficiency, and (c) safety concerns. The favored alternative to these two storage methods is natural gas adsorbed on a microporous medium such as highly porous carbon.

Natural gas contains portions of ethane, propane, and butane, but the main component is methane. As such, research has focused on finding a porous material that can store adsorbed methane. Theoretical studies have shown that an optimal material engineered to enhance capillary condensation and gas adsorption would possess pores 1.5–2.5 nm in diameter and a pore volume in this range of greater than 1 cc/g [237]. Activated carbon is the dominant material in this field because of its ease of processing and

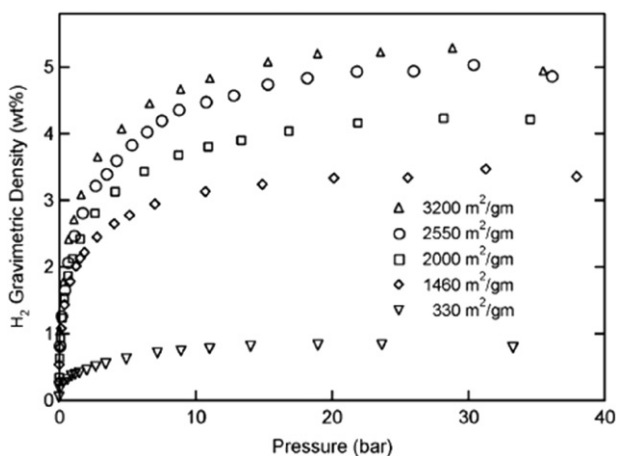


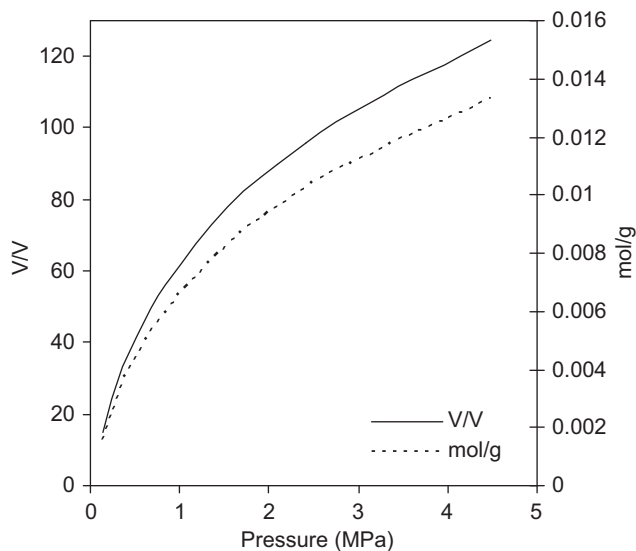
**Figure 9** Adsorption isotherms at 77 K for the carbon aerogels show the linear dependency of hydrogen adsorption on the surface area [233].

controllable pore structure. Other types of porous materials could be used, such as metal organic framework (MOF) materials. These also contain tunable micropores (defined by IUPAC as pores <2 nm in diameter), but most work has been focused on activated carbons [238]. The bulk of the literature focuses on pyrolysis (or carbonization) and activation treatments on existing organic materials such as pitch, coconut fibers [239], pistachio nut shells [240–243], carbon fibers [244], and even tire rubber [245].

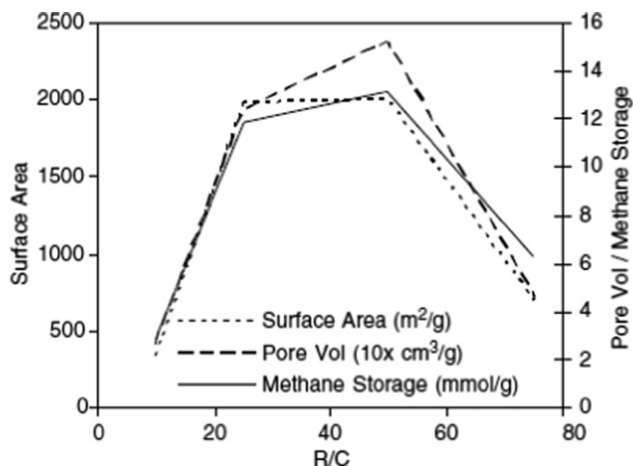
Fig. 10 shows the typical methane adsorption curves of a resorcinol-formaldehyde carbon cryogel at room temperature [222], with volumetric and gravimetric storage as a function of pressure measured using a Sievert's apparatus [246]. Volumetric storage capacity is not a material property as it largely depends on sample compaction, but the gravimetric storage capacity is indicative of the microporous structure of the sample in question. The methane sorption curves in these carbon cryogels are similar to that of activated carbon widely reported in literature [247–249].

Fig. 11 shows that the gravimetric storage capacity varies as a function of *R/C* (precursor resorcinol to catalyst sodium carbonate) ratio. For example, increasing the *R/C* value from 10 to 25 resulted in a drastic increase in methane storage capacity (~4 times), which reaches its maximum of 13 mmol/g at *R/C*=50, and then decreases significantly as the *R/C* ratio increases further to 75. Total pore volume and surface area are also plotted in Fig. 11, showing a close correlation between all three metrics. This can be easily understood when considering the fact that methane storage in carbon cryogels occurs in two mechanisms: surface adsorption (both monolayer and multilayer adsorption) and capillary condensation in micropores.

An *R/C* value either too high or too low is not beneficial for the storage performance of the material. Pekala [250] has shown by small angle X-ray scattering (SAXS) analysis that in the RF system, the length scale of the solid and solvent phases in the gelling RF polymer network are equal and dependant on *R/C*. At low *R/C* ratios, the width of both the pores and solid phases are very small whereas high



**Figure 10** Methane adsorption curves in terms of V/V and mol/g for a carbon cryogel at room temperature.



**Figure 11** Gravimetric (mmol/g) methane storage performance, surface area ( $\text{m}^2/\text{g}$ ), and total pore volume ( $10 \times \text{cm}^3/\text{g}$ ) as a function of  $R/C$  for carbon cryogels and activation levels from 67% to 75% [222].

$R/C$  ratio results in an open structure with large pores and correspondingly large solid portions. Hence, a high  $R/C$  carbon cryogel exhibits poor methane storage capacity because the material consists of large solid chords of carbon separated by pores of an equal size, larger than that is beneficial. Poor performance in low  $R/C$  cryogels may be explained by drying or pyrolysis induced collapse of the very small pores that result from the highest catalyst concentrations. Related behavior such as reduced micropore volume and surface area at high or low  $R/C$  ratio has been noted in the literature [251].

This study appears to be the first attempt to use carbon cryogels (or aerogels) for pressurized gas storage. The initial results are promising, but there is still considerable room for extensions of this work. Relatively few publications have reported on the properties of activated carbon aerogels [248,252]. Further understanding of this system, and possibly utilizing alternate activation temperatures, would enable better control over the final material properties.

### Carbon-based nanocomposites for hydrogen storage

It is well recognized that hydrogen generated from renewable power represents a very attractive energy solution. Hydrogen powered fuel cells are more efficient than internal combustion engines and have only water as an emission. Unfortunately, hydrogen storage systems suitable for automotive and other small-scale industrial or residential applications remain elusive. Using ultra-high pressure (860 bar) or ultra-low temperatures (30 K) continue to be the only methods for achieving sufficient and commercially practical storage densities [253,254]. This significant constraint is a well-known, yet persistent, obstacle to widespread implementation of a hydrogen economy. Currently, a variety of solid state hydrogen storage materials are the subject of intensive investigation and research. However, no material has yet to meet simultaneously all of the following criteria [255]: relatively high storage density of 3 kWh/kg at 9 wt% and 2.7 kWh/L, moderate decomposition tempera-

tures of 60-120 °C, good reversibility, low manufacturing cost that can support \$2/kWh end-use pricing, and fast kinetics of the hydrogen absorption and desorption process.

The concept of a dual phase coherent nanocomposite hydrogen storage material has been developed and studied, where the two phases consist of highly porous carbon and hydride hydrogen storage material [249,256-259]. Porous carbon with a high surface area and pore volume would contribute significantly to a solid state hydride-based hydrogen storage composite material by providing a structural support matrix, as well as size confinement for hydrides and a percolated heat conduction network.

Incorporation of  $\text{LiBH}_4$  into carbon aerogels (CAs) has shown to enhance the dehydrogenation kinetics and lower the dehydrogenating temperature of  $\text{LiBH}_4$ . Fig. 12 shows the thermo-gravimetric analysis for hydrogen release from  $\text{LiBH}_4$  confined in two aerogels with pore sizes of 13 and 26 nm, activated carbon with pore sizes of  $<2$  nm, and a non-porous graphite control sample [260]. This study shows that incorporation of  $\text{LiBH}_4$  into the CA accelerates the dehydrogenation, reduces the energy barrier to release hydrogen, and decreases the hydrogen release temperature, with lower dehydrogenation temperature observed for CA with smaller pore size.

Fig. 13 is a schematic illustrating the coherent nanocomposite of ammonia borane (AB) within a carbon cryogel network. AB was chosen as a hydride material for its high gravimetric and volumetric hydrogen content, as well as its already reasonable decomposition temperature. AB is also easily coated onto the carbon cryogel by dissolving it in solvent and soaking the cryogel, resulting in a coherent nanocomposite, as illustrated in Fig. 13. The addition of AB to the carbon cryogel resulted in hydrogen release at a much lower temperature and the elimination of harmful byproducts.

Carbon cryogel (CC)-ammonia borane (AB) nanocomposites can be made by loading monolithic CCs with AB through soaking them in AB/THF solution [261,262]. The DSC exotherms for CC-ABs and neat AB are given in Fig. 14a. Thermal decomposition of neat AB happens through two-step reactions, which were observed at approximately

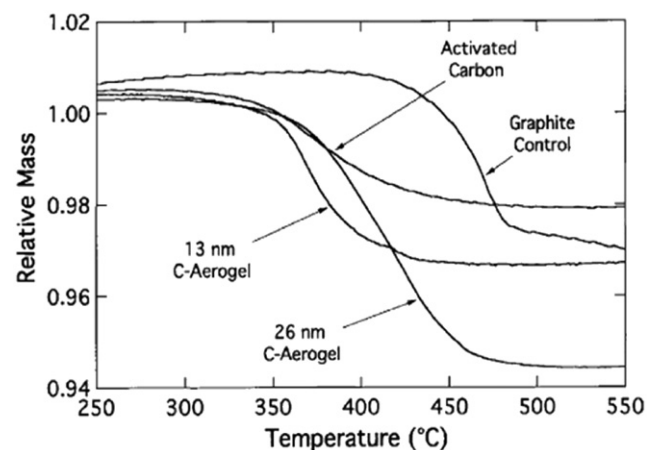


**Figure 12** Thermogravimetric analysis of  $\text{LiBH}_4$  dehydrogenation shows that the reaction temperatures decrease with the decreasing scaffold pore size [260].

115 and 150 °C at the applied heating rate. These temperatures are in good agreement with the literature [263]. Similar results were reported in other nanocomposites, including mesoporous silica-AB [264] and carbon aerogel-LiBH<sub>4</sub> [260]. For the CC-AB nanocomposites, dehydrogenation temperatures are much lower than that of neat AB and hydrogen release happens through only one exothermic event. For the CCs with pore sizes of 7, 9, and 16 nm, dehydrogenation temperatures are ~98, 102, and 110 °C, respectively. Lower dehydrogenation temperatures in CC-ABs provide evidence of faster kinetics. The dehydrogenation of nanocomposites is very reproducible and results in the release of about 1.5 H<sub>2</sub> equiv and suppression of borazine. Also, the reaction exothermicity is significantly more than that of neat AB [261]. <sup>11</sup>B nuclear magnetic resonance and FTIR studies showed the lower dehydrogenation temperature and enhanced kinetics in the thermal reaction of CC-AB is accompanied by the formation of a new reaction product, which is attributed to the reaction of AB with surface oxygen functional groups [265]. It should also be noted that the dehydrogenation occurred at a much narrower range of temperatures. Although the exact mechanism for narrowed dehydrogenation peaks is still under research, it is likely due to the better thermal

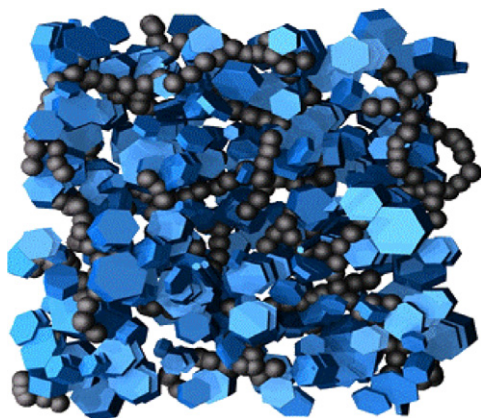


**Figure 13** Illustration of the anticipated structure of a coherent nanocomposite consisting of a carbon cryogel network and hydride [261].

conductivity of the nanocomposites and the consequent rapid kinetics as compared to the neat AB. The peak dehydrogenation of CC-ABs and their corresponding CC pore size are compared in Fig. 14b, which reveals that the dehydrogenation temperature decreases almost linearly with the pore size.

Activation energies are calculated for non-isothermal DSC runs using the Kissinger equation [266], given by

$$\ln(\alpha/T_p^2) = -E_a/RT_p + C \quad (5)$$

where  $T_p$  is the peak temperature,  $\alpha = dT/dt$  the heating rate,  $E_a$  the activation energy, and  $C$  the intercept. The plot of  $\ln(\alpha/T_p^2)$  versus  $1/T_p$  is linear and the slope of the resulting line corresponds to the values of the activation energy from the Kissinger equation. Table 1 shows the peak temperatures for heating rates of 2, 5, and 10 °C/min. The calculated activation energy for neat AB is about 160 kJ/mol, which is comparable to the value reported in literature using the isothermal method [264]. The activation energies for nanocomposites are lower than that of neat AB: about 150 kJ/mol AB and 120 kJ/mol AB for 16 nm-CC-AB, and 7 nm-CC-AB. Similar to the dehydrogenation temperatures, the activation energies decrease with the decrease in pore size. These results suggest that the barrier for hydrogen release from CC-ABs is lower than that of the neat AB.

The dehydrogenation temperature and kinetics of ammonia borane on pore size in amorphous nanoporous carbon-ammonia borane nanocomposites vary appreciably with the change in pore size of the CC scaffold. Confining nanocrystallite AB inside the mesopores of the carbon matrix decreases the dehydrogenation temperatures and activation

**Table 1** Peak temperatures for dehydrogenation of AB and CC-AB [262].

Heating rate (°C/min)	AB $T_p$ (°C)	16 nm CC-AB $T_p$ (°C)	7 nm CC-AB $T_p$ (°C)
10	124	115	109
5	118	109	101
2	112	103	94
$E_a$	160 kJ/mol	150 kJ/mol	120 kJ/mol

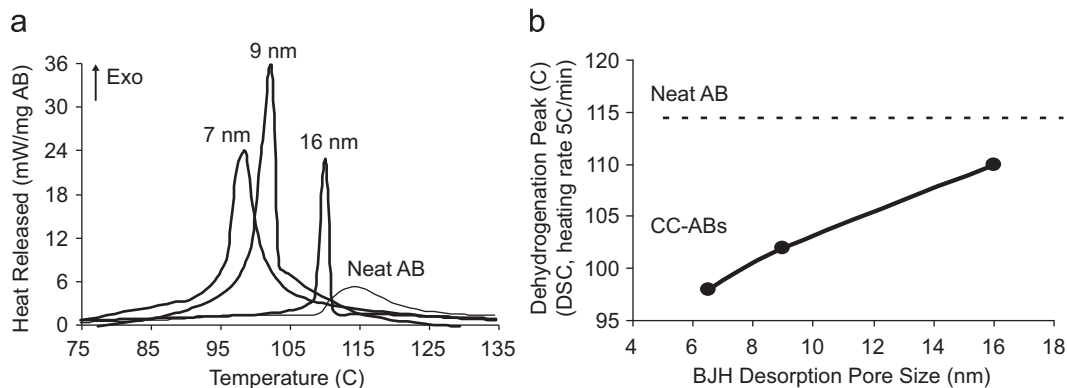


**Figure 14** (a) DSC exotherms for CC-AB nanocomposites at a heating rate of 5 °C/min and (b) comparison of dehydrogenation peaks for CC-AB nanocomposites for corresponding CC pore sizes. The dashed line shows the dehydrogenation temperature for AB at a similar heating rate [262].

energy. The carbon matrix reduces hydrogen diffusion distances, increases the frequency of reaction, which effectively accelerates the dehydrogenation process, and serves as efficient pathways for heat transfer. Inside the mesopores of the CC matrix, nanocrystallite AB possesses a huge surface to volume ratio, resulting in significantly larger surface energy. This destabilizes the hydrogen bonding network of AB and lowers the barrier to hydrogen release. Other possible factors, such as surface area and catalysts, for dehydrogenation temperatures and the kinetics of hydrides have also been studied; boron and nitrogen modified CCs (BNCCs) have been shown to enhance kinetics and lower dehydrogenation temperatures further.

Fig. 15 shows the DSC exotherms (at 5 °C/min) for AB, CC-AB, and BNCC-AB nanocomposites. Thermal decomposition of AB shows an endothermic dip at approximately 105 °C (assigned to the melting of AB) and two exothermic maxima, one at approximately 115 °C and a smaller one ~150 °C, associated with the release of the first and second equivalent of hydrogen, respectively [263,268]. The activation energy for release of the first equivalent of hydrogen from neat AB is found to be ~160 kJ/mol, which is comparable to the value reported in literature [269]. The activation energies for nanocomposites are ~150 kJ/mol AB and 115 kJ/mol AB for CC-AB and BNCC-AB, respectively.

The lower dehydrogenation temperatures and activation energies of CC-AB and BNCC-AB can be attributed to the size dependent surface energy of AB confined inside the nanoscale pores of CC and BNCC. The carbon matrix can reduce hydrogen diffusion distances, increase the frequency of reaction, which effectively accelerates the dehydrogenation process, and serve as efficient pathways for heat transfer. Thus, the barrier to hydrogen release in CC-AB and BNCC-AB is lower. Also, the surface hydroxyl groups may result in the catalysis of the AB thermal reaction in nanocomposites. Furthermore, the lower activation energy and dehydrogenation temperature in BNCC-AB than CC-AB can be attributed to the catalytic effect and not the nanoscale effects. The presence of B, N, and the excess of hydroxyl groups on the surface BNCC can provide surface interactions that disrupt the dihydrogen bonding in AB. Therefore, the induction period for dehydrogenation is

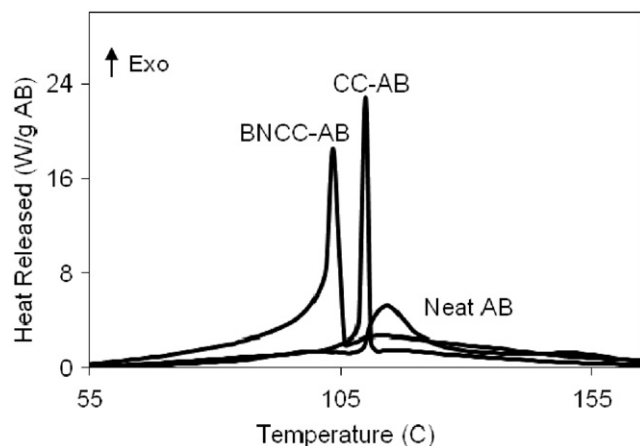


**Figure 15** DSC exotherms for CC-AB and BNCC-AB nanocomposites and neat AB (heating rate 5 °C/min) [267].

lower, resulting in a lower barrier to hydrogen release in BNCC-AB as compared to CC-AB.

It should be noted that the nanosize confinement has also been observed in silica-ammonia borane nanocomposites. It has been shown that infusing ammonia-borane (AB) in a nanoporous silica scaffold lowers the activation barrier for the hydrogen release, significantly improves the dehydrogenation kinetics, lowers the dehydrogenation temperature, and suppresses unwanted volatile products [264].

## Porous nanostructured carbon materials for fuel cell application

Porous carbon is the indispensable material in fuel cells (e.g., polymer electrolyte membrane (PEM) fuel cell) [270]. In a PEM fuel cell, porous carbon is the most widely used electrocatalyst support material [271-273] and can even be used as electrocatalyst with a certain functional group [274-276]. It is the basic material in the gas diffusion layer [277,278] and it is also incorporated into composite membranes to enhance their mechanical strength [279]. In this section, we will focus on the electrocatalytic application of porous carbon.

### Electrocatalyst support

Most PEM fuel cell electrocatalysts are Pt (Pt alloy) nanoparticles supported on porous materials. The support materials play a key role in improving Pt utilization, catalytic activity, and stability. The general requirements for electrocatalyst support are [272] (1) high specific surface area and high porosity, which are necessary for improving the dispersion of catalytic metals and mass transfer; (2) high electrochemical stability under fuel cell operating conditions; (3) high electric conductivity; and (4) easy Pt recycling in the used electrocatalyst. The special interaction between Pt and the support material is also desired to improve the catalytic activity and durability of Pt [280-282]. Porous carbon intrinsically possesses these unique properties. Vulcan XC-72 carbon black is the most widely used electrocatalyst support, but the activity and durability do not satisfy the requirements for PEM fuel cells. Therefore, various nanostructured carbon materials have been developed for electrocatalyst supports [272], including carbon nanotubes (CNT), mesoporous carbon, the newly developed graphene, etc.

CNTs are superior to conventional carbon black for PEM fuel cell electrocatalyst support in many ways [272,283-286]: (1) CNTs are more electrochemically durable in fuel cell conditions; (2) CNTs provide a high electric conductivity and a specific interaction between Pt and CNT support (i.e., the interaction of the delocalized  $\pi$ -electrons of CNTs and Pt d-electrons), resulting in a higher catalytic activity; (3) CNTs have few impurities, while carbon black (e.g., Vulcan XC-72) contains a certain quantity of impurities, such as sulfur, which poison Pt metal; (4) CNTs are free from the deep-crack structure, which is the so-called “dead zone” of electrocatalysts because Pt nanoparticles have no catalytic activity when deposited there due to the absence of electrochemical triple-phase boundary. Various CNTs have been developed for fuel cell electrocatalyst supports.

Usually CNTs with smaller diameters exhibit higher specific surface area, which is beneficial for the dispersion of Pt nanoparticles and results in high electrocatalytic activity. It has been reported [287,288] that single wall carbon nanotubes (SWNT) [287,288] and double wall carbon nanotubes (DWNT) [289,290] supported Pt/Pt alloy electrocatalysts show better activity toward methanol oxidation [287-289] and oxygen reduction [290] than those supported by multi-wall carbon nanotubes (MWNTs) [287,288]. In addition to the diameter of CNTs, the nanostructures of CNTs also influence the electrocatalytic performance [291,292]. For example, bamboo-structured MWNTs, in which the axis of the graphite planes is at an angle to the axis of nanotubes, show faster electron transfer in electrochemical processes than hollow-structured MWNTs [293]. The higher electrocatalytic performance of bamboo-structured MWNTs has been observed for the reduction of oxygen [294] and  $H_2O_2$  [295]. These enhanced electrocatalytic activities are attributed to the greater proportion of edge plane-like defect sites in bamboo-structured MWNTs [294-296].

Mesoporous carbon (MC) is another material that has been extensively studied as catalyst supports for PEM fuel cells [25,297-302]. The performance of the mesoporous carbon supported electrocatalysts is influenced by both the pore structures and sizes. Extensive studies have been carried out on the influence of the pore size of support on electrocatalytic activity [299,303,304]. The highest performance was found for the porous carbon with mesopores (20-25 nm) as the support [299,303,304]; this exhibits the balance among high surface area, which allows a higher degree of catalyst dispersion, pore size, which allows for efficient transport of reactants and products, and electric conductivity [302].

Graphene is a newly developed carbon material, which has shown both enhanced activity and durability as fuel cell catalyst support [280,305,306]. Graphene has been observed to exhibit an extraordinary modification to the properties of Pt cluster electrocatalysts supported on it, which leads to an electrocatalytic activity enhancement by a factor of 4 for methanol oxidation [280]. Fig. 16 shows Pt subnano-clusters (<0.5 nm) formed on graphene due to the specific interaction between Pt and the graphene surface, which in turn acquires the specific electronic structures of Pt and modifies its catalytic activities [280]. Graphene also improves the stability of Pt electrocatalysts. Less aggregation of Pt nanoparticles on the functionalized graphene and

higher retained activity of Pt/graphene in comparison with Pt on carbon black have been observed under durability tests [306].

To improve the durability of electrocatalysts through carbon supports, generally two strategies have been employed [272]: (1) graphitization of porous carbon and (2) surface modification of carbon support with corrosion-resistant conductive metal oxides. In a PEM fuel cell, the carbon catalyst support can be corroded, which leads to degradation of the electrocatalysts. The electrochemical corrosion rate mainly depends on the degree of graphitization in the carbon [272]. It has been demonstrated that increasing the degree of graphitization, for example, through high-temperature heat treatment in inert atmosphere, can improve the durability of electrocatalysts [307,308]. However, the high-temperature heat treatment usually significantly decreases the surface area and the anchoring sites for Pt, which makes it difficult to load highly dispersed Pt nanoparticles [307,309]. Another strategy is to modify the carbon support surface with a protective layer like conductive metal oxides. In fact, this protective layer not only improves carbon durability, but also stabilizes Pt nanoparticles through the strong metal-support interaction. Furthermore, the metal oxide (indium tin oxide, ITO), carbon, and platinum can form a triple-junction structure as shown in Fig. 17, which significantly improves both the activity and the durability of the electrocatalyst [305].

### Porous carbon based non-precious electrocatalysts

Porous carbon, if functionalized with other elements like nitrogen [274,275] and transition metals [276], can be used as electrocatalysts by itself, which is referred to as non-precious electrocatalyst. This is a strategic direction in fuel cell research to replace expensive platinum.

Nitrogen doping of porous carbon has been used as a strategy to improve the activity and durability of carbon supported precious metal electrocatalysts [275], but the catalytic activity of nitrogen-doped carbon itself has never been able to compete with platinum until Gong et al. [274] successfully demonstrated the superior activity of their nitrogen-doped carbon nanotubes array (N-CNT). The N-CNT exhibits a comparable activity and much higher durability and selectivity in comparison with platinum for oxygen reduction in alkaline electrolyte [274]. However, this

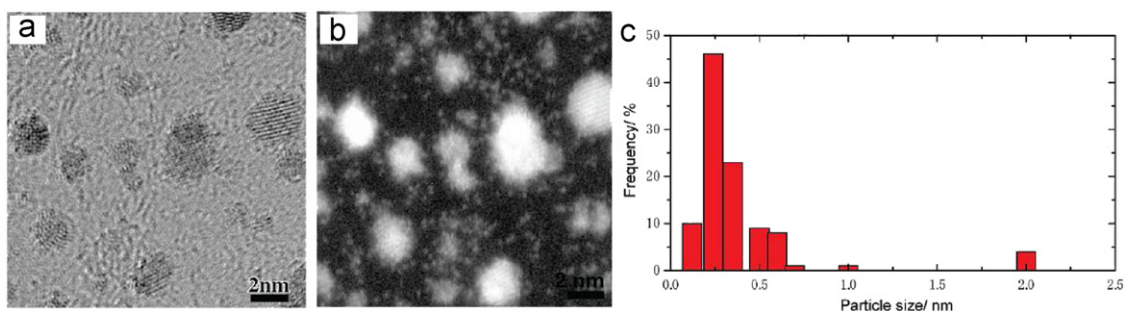


**Figure 16** (a) HRTEM image and (b) HAADF-STEM image of Pt/graphene. (c) Histogram of subnanometer sized Pt clusters of Pt/graphene (HAADF-STEM=high-angle-annular-dark-field-scanning-transmission electron microscope) [280].

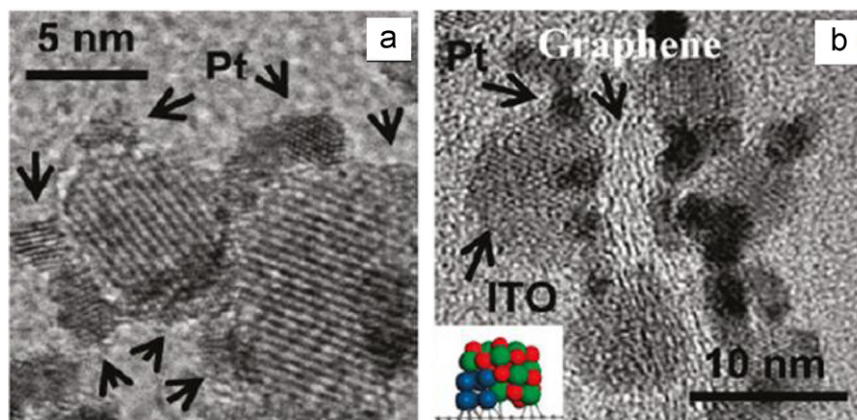


Figure 17 (a) Face-on and (b) cross-sectional TEM images of Pt/ITO-graphene [305].

superior performance of the nitrogen-doped carbon has not been demonstrated in acidic electrolyte, which is more important for practical application since most low-temperature fuel cells are acidic systems. Fortunately, great progress has been made by incorporating transition metals (Fe, Co, etc.) to improve the electrocatalytic performance of carbon based non-precious catalysts in acidic systems [276,310,311]. Lefèvre et al. [310] reported that their microporous carbon/iron-based catalysts could produce current densities equal to that of a platinum-based electrode with a Pt loading of  $0.4 \text{ mg/cm}^2$  at a cell voltage of  $\geq 0.9 \text{ V}$ , but the durability is still poor (a decrease by about 50% in 100 h test). Wu et al. [311] recently reported a highly stable porous carbon/iron/cobalt-based non-precious electrocatalyst with a slightly lower activity than Pt. Their most active materials catalyze oxygen reduction at potentials within  $\sim 60 \text{ mV}$  of that delivered by state-of-the-art carbon-supported platinum. The stability is remarkable with almost no degradation in 700 h at a fuel cell voltage of  $0.4 \text{ V}$  [311]. These are exciting results in the search for non-precious electrocatalysts even though more investigations are needed to understand the fundamental mechanisms, which will lead to highly active and stable non-precious electrocatalysts.

### Porous carbon for solar cell applications

Using various porous carbon materials such as CNTs, graphene, fullerenes, mesoporous carbon, and other fabricated hollow nanoparticles can be beneficial for cell performance in dye-sensitized solar cells (DSSCs), quantum-dot sensitized solar cells (QDSCs), and organic solar cells [312-321]. For example, DSSCs showed an improved conversion efficiency of 7.46% using ordered mesoporous carbon with a high surface area ( $\sim 1575 \text{ m}^2/\text{g}$ ) as the counter electrode [317]. The large area, flexible, transparent, and conductive carbon films made by spinning or depositing can be transferred to various substrates such as glass, metal, paper, plastics, and micro-fibers.

Porous carbon-based composite materials are also attractive when used as transparent electrodes, counter electrodes, electrolytes, and other parts in the solar cell. For improved photoelectronic properties, various carbon-based

composites were synthesized and studied, such as the mixture of graphene, CNTs, and ionic liquid as electrolytes [313],  $\text{TiO}_x$ -modified CNTs as transparent electrodes [314], Pt-decorated CNTs as the catalytic layer on counter electrodes [322], and  $\text{TiO}_2$  NPs/CNTs hybridized material as working electrodes [323], as well as polymer/CNTs [324,325], reduced graphene-CNTs [326], P25-graphene [327], and TiN-CNTs composites [328] as counter electrodes. The efficiency of the DSSCs using most composites as counter electrodes is comparable to that with a Pt film electrode. Instead of spinning or depositing CNTs on substrates, ordered CNT arrays grown on FTO glass and graphene paper (Fig. 18a) were also synthesized and used as the counter electrode [329,330], as it was believed that the aligned structures would provide faster electron transfer and thus more stable performance. Additionally, Lee et al. prepared N-doped CNT arrays as electrodes with an excellent conversion efficiency of 7.04% in DSSCs [331]. Zhou et al. synthesized amorphous silicon (a-Si:H) capped CNT arrays (Fig. 18b) with a 25% enhancement in short circuit current attributed to the highly effective light-trapping structure of the coaxial MWNT/a-Si:H nanowire array [332].

Many researchers focus on the design of CNTs-silicon heterojunction solar cells for achieving high efficiency by enhancing photon absorption, inhibiting charge recombination, and reducing internal resistance. For example, Ong et al. prepared hybrid solar cells based on SWNTs/Si heterojunctions [333], while Kalita et al. incorporated CNTs into silicon nanowire (SiNW) arrays/polymer hybrid solar cells [334]. Shu et al. fabricated a hybrid solar cell composed of a heterojunction cell and a photoelectrochemical (PEC) cell [335]. A thin CNTs film formed a heterojunction with the SiNWs and also functioned as the transparent electrode. The cell structure is shown in Fig. 19. The hybrid solar cell showed a power conversion efficiency of 1.29% under AM 1.5G illumination, higher than those for SiNW arrays-based PEC cells. Jia et al. reported Si-CNT heterojunction solar cells with a stable high efficiency of 10-13% by acid doping [336,337].

### Porous carbon for lithium-sulfur batteries

Mesoporous carbon (MC) with large surface area, good conductivity, and tunable pores is an ideal conductive

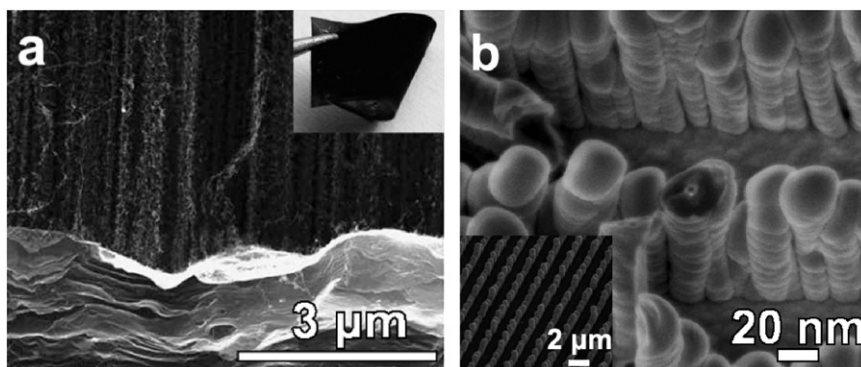


**Figure 18** SEM images showing (a) the cross section of CNTs grown on graphene paper with an optical image inserted in the top right corner [330] and (b) the CNTs capped with amorphous silicon with low magnified image inserted in the lower left corner [332].

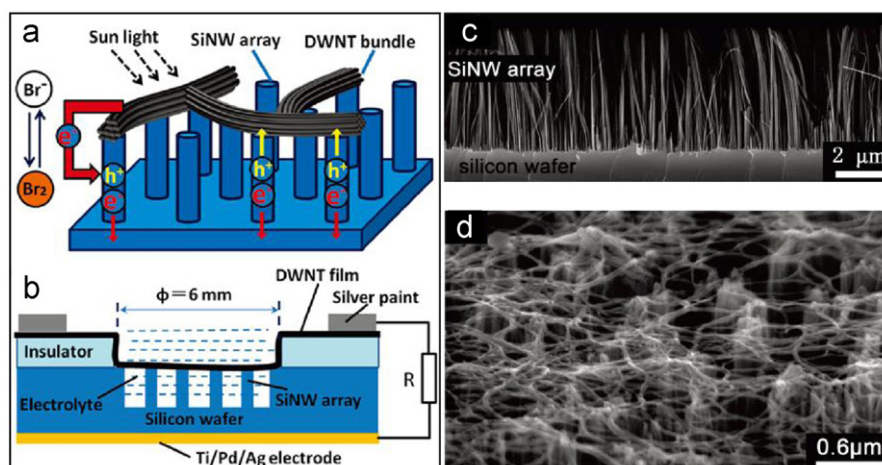


**Figure 19** (a) Schematic illustration of a hybrid heterojunction/PEC solar cell made with CNTs and SiNW arrays and (b) side view of the structure. (c) Cross section of the obtained SiNW array on the silicon wafer and (d) top view showing CNTs on top of the SiNW array [335].

matrix for electrical energy storage applications. Trapping active materials inside the pores leads to composite battery electrodes with improved capacity, cycling stability, and rate capability. Li-S batteries have high theoretical specific capacity ( $\sim 1680 \text{ mAh g}^{-1}$ ) and energy density ( $2600 \text{ Wh/kg}$ ), but suffer from the poor electrical conductivity of sulfur and the fast capacity degradation from polysulfide dissolution into the electrolyte [338–341]. Recently, mesoporous carbon has been used to construct cathodes for Li-S batteries by encapsulating sulfur inside the pores [341–344]. A mesoporous carbon-sulfur (MCS) composite improves the electrical conductivity of the sulfur cathode and alleviates the fast capacity degradation from polysulfide dissolution into the electrolyte. Using sulfur and ordered MC (CMK3) nanocomposites as cathodes for Li-S batteries, good cycle stability of over 20 cycles and high initial discharge capacities of  $\sim 1320 \text{ mAh g}^{-1}$  and  $1005 \text{ mAh g}^{-1}$  were achieved at a 0.1C rate ( $168 \text{ mA/g}$ ) with and without polyethylene glycol (PEG) modification, respectively (Fig. 20) [344]. Bimodal MCs and porous hollow carbon spheres prepared using soft or hard templates have been reported [342,343]. An ordered MC with a large surface area ( $2102 \text{ m}^2/\text{g}$ ), a pore volume of  $2.0 \text{ cm}^3/\text{g}$ , and a bimodal mesoporous structure (5.6/2.3 nm) has been synthesized using the tri-constituent co-assembly method. With 60 wt% sulfur loading, the composite

has an initial capacity of  $\sim 1100 \text{ mAh g}^{-1}$  and a capacity retention of  $\sim 800 \text{ mAh g}^{-1}$  after 80 cycles [340]. Another bimodal MC (2/7.3 nm), synthesized using a soft-template approach and KOH activation, has a relatively small pore volume ( $0.56 \text{ cm}^3/\text{g}$ ) and a maximum sulfur loading of 37.1 wt%. A capacity retention of  $\sim 700 \text{ mAh g}^{-1}$  over 50 cycles was obtained with 11.7% sulfur loading [342]. Porous hollow carbon spheres, with an interior void space and a mesoporous shell structure, exhibited extended cycling for 100 cycles with  $\sim 950 \text{ mAh g}^{-1}$  capacity retention at a high current density of about  $850 \text{ mA/g}$  [343].

To achieve high energy density in Li-S batteries, MC with large pore volume and full sulfur filling is desired. However there is a dilemma between the sulfur utilization, cycling stability, and sulfur loading. High sulfur loading and full sulfur filling will result in low sulfur utilization and fast capacity fading. The performances of a series of MCS composite electrodes were investigated. It was found that at full sulfur-filling conditions, the MC pore structure (pore sizes and volumes) has no influence on battery performance other than increasing the maximum sulfur loading for increased pore volume.

MC with tunable pore sizes (22, 12, 7, and 3 nm) and pore volumes (from 1.3 to  $4.8 \text{ cm}^3/\text{g}$ ) are synthesized using a hard template approach [345]. The electrochemical

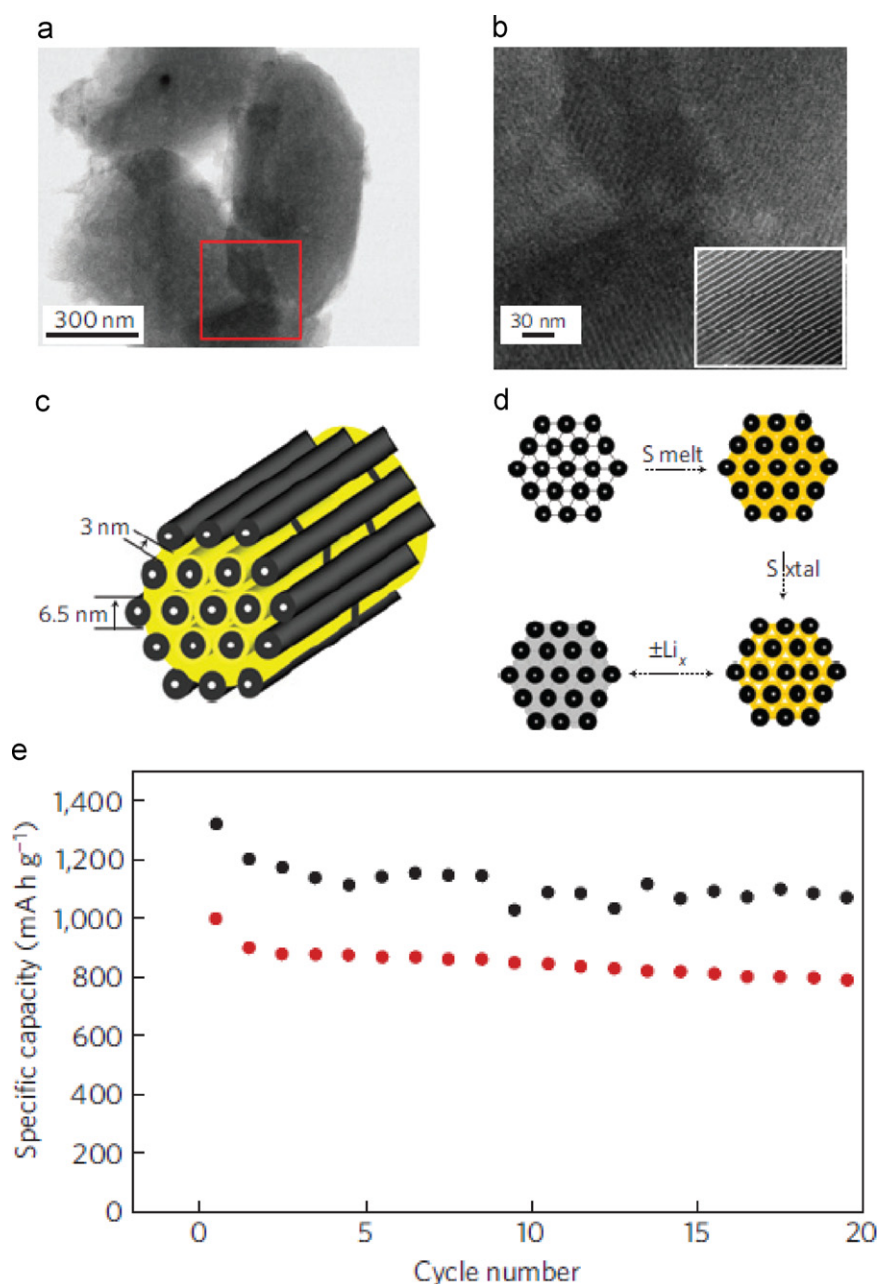


**Figure 20** Mesoporous carbon as a host for S encapsulation [344]. (a) and (b) TEM images of mesoporous carbon. (c) and (d) Schematic illustration and procedure for S encapsulation. (e) Specific capacity as a function of charge/discharge cycles (dark cycles: polymer coated; red cycles; no coating).

performances of MC22, MC12, MC7, and CMK3 with full sulfur filling are compared in Fig. 21. Fig. 21a shows typical first charge-discharge profiles of these MCS composites, which exhibit similar features. The first discharge capacities for all MCS composites are similar,  $\sim 1100 \text{ mAh g}^{-1}$ , suggesting that sulfur utilization at full sulfur-filling conditions is close to each other based on their similar percentage from the theoretical capacity of about  $1680 \text{ mAh g}^{-1}$ . Fig. 21b shows the long-term cycle performance of MC22, MC12, MC7, and CMK3 at a current density of  $168 \text{ mA/g}$  ( $0.1 \text{ C}$ ). In spite of the very large differences in sulfur loading (from 56 to 83 wt%), the cycling stabilities of these MCS composites are also similar, exhibiting a capacity retention of  $\sim 600 \text{ mAh g}^{-1}$  after 50 cycles.

To achieve MCS composite electrodes with high sulfur utilization and prolonged cycle stability, efforts need to focus on (1) improving the interface between sulfur and the MC and (2) curbing the dissolution/diffusion of polysulfide anions into the electrolyte, as sulfur filling inside the mesopores ensures that sulfur nanoparticles are electrically well connected to the conductive frame. One simple method is to use an MCS with partial sulfur filling. The decrease in sulfur loading leads to better sulfur dispersion inside the MC mesopores, which improves the relative amount of sulfur particles at the interface with the MC. Hence, the electrochemical reaction degree is improved. Furthermore, a fraction of surface area and pore volume is still accessible in the mesopores of the partially filled MC. The unoccupied

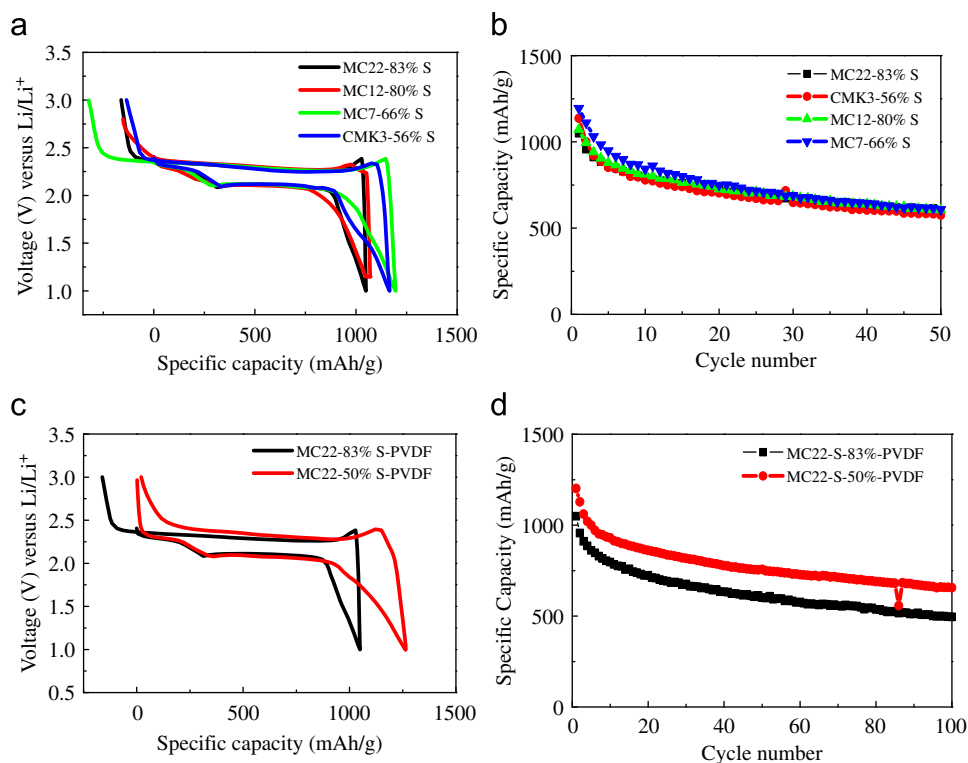


**Figure 21** Battery performance of the MCS composite electrodes. (a) First cycle charge-discharge profiles of MC22, MC12, MC7, and CMK3. (b) Cycle performance of MC22, MC12, MC7, and CMK3. (c) First cycle charge-discharge profiles of MC22-83 and MC22-50. (d) Cycle performance of MC22-83 and MC22-50.

space inside the mesopores provides a nano-environment that confines the dissolved polysulfide anions and the reaction products in the local proximity of the cathode surface, and makes them available for further electrochemical reactions. A high sulfur utilization (initial capacity) and prolonged stable cycling will be obtained.

MCS composites with partial sulfur-filling were designed to validate the above understanding. An MC with a large pore volume should be used in the synthesis of these partially filled MCS composites in order to concurrently have practical sulfur loadings and enough empty volume within the pores. MC22 with 50 wt% sulfur loading was prepared and tested as a cathode for Li-S batteries. The sulfur is very well dispersed in the MC, filling part of the total mesopore volume. As expected, improved battery performance was obtained using MC22-50 as the cathode in Li-S batteries. Fig. 21c exhibits a discharge capacity of  $\sim 1250 \text{ mAh g}^{-1}$ , corresponding to 74.6% sulfur utilization based on the theoretical capacity of  $1675 \text{ mAh g}^{-1}$ . Long-term cycling of an MC22-50 based electrode also shows significant improvement with capacity retention of  $\sim 650 \text{ mAh g}^{-1}$  over 100 cycles (Fig. 21).

Observations from the MCS composite at full sulfur-filling conditions are also supported by results recently reported by other groups [342]. For example, the design of bimodal porous carbon uses the micropores to contain the sulfur and large pores to provide space for electrolyte diffusion [345]. Conclusions on the selection of MC materials and control of the sulfur-filling level apply regardless of differences in the carbon structures. The sulfur content loaded in the pores has to be tailored to a practical loading level that is below the maximum limit calculated from the pore volume of the

MC material. An MC with a large pore volume should be chosen to maximize the deliverable capacity because although the level of sulfur loading has to be lower than the maximum theoretical loading, the structure should nevertheless contain as much sulfur as possible.

Many other porous materials have also been investigated for Li-S application. For example, a functionalized graphene sheet-sulfur (FGSS) nanocomposite was synthesized as the cathode material for Li-S batteries [346]. The structure has a layer of functionalized graphene sheets/stacks (FGS) and a layer of sulfur nanoparticles, creating a three-dimensional sandwich-type architecture. This unique FGSS nanoscale layered composite has a high loading (70 wt%) of active material (S), a high tap density of  $\sim 0.92 \text{ g/cm}^3$ , and a reversible capacity of  $\sim 505 \text{ mAh g}^{-1}$  ( $\sim 464 \text{ mAh/cm}^3$ ) at a current density of  $1680 \text{ mA/g}^1$  (corresponding to 1 C rate). When coated with a thin layer of cation exchange Nafion film, the migration of dissolved polysulfide anions from the FGSS nanocomposite was effectively reduced, leading to a good cycling stability of 75% capacity retention over 100 cycles. This sandwich-structured composite conceptually provides a new strategy for designing electrodes in energy storage applications.

## Porous carbon for lithium oxygen batteries

An important application of porous carbon is the construction of air electrodes for various metal air batteries [347]. Unlike conventional batteries, metal air batteries store the active material, oxygen, in the environment. The open

structure design of the metal air batteries “pumps” in the oxygen on demand and releases oxygen back into the environment during charging; therefore the energy density from this system is much higher than that of other rechargeable batteries [347,348]. Among all kinds of metal air systems, lithium air batteries or lithium oxygen batteries, depending on the oxygen partial pressure during testing, have attracted extensive attention recently [349]. Fig. 22a represents a typical structure of a rechargeable Li-oxygen battery [350]. Because oxygen has to be supplied into the interior carbon during discharge, the design of appropriate porous structures for the carbon electrode becomes important in this system. The air electrode in Fig. 22 consists of dominantly carbon and a small amount of binder such as polytetrafluoroethylene (PTFE). The porous carbon electrode not only supplies electrons continuously for the electrochemical process but also provides numerous solid-liquid-gas tri-phase regions for the oxygen reduction. The pores and the surface of the carbon electrode are also the host of the  $\text{Li}_2\text{O}_2$  discharge product [351]; thus they play a key role in determining the overall electrochemical performances of the Li- $\text{O}_2$  batteries and will be discussed in detail.

The surface area of porous carbon is related to the performance of Li- $\text{O}_2$  batteries because a larger surface area means more active sites for electrochemical reactions and also more catalysts can be loaded onto the porous carbon. However, detailed studies on the relationship between surface area and the capacity delivered from Li- $\text{O}_2$  batteries reveal that higher surface area does not always lead to a higher capacity. Instead, the discharge capacity is largely determined by the pore volume of the carbon, especially the amount of mesopores [352,354,355]. For example, Ketjen black has the highest total pore volume of 7.6 cc/g, most of which is contributed from mesopores. The air electrode made from Ketjen black exhibited much higher capacity than any other commercial carbons under the same measurement conditions. In the same pure oxygen environment, activated carbon (AC) with the highest surface area (2100  $\text{m}^2/\text{g}$ ) shows much lower capacity than Super P, whose surface area is only 62  $\text{m}^2/\text{g}$  but has a large pore diameter of 50 nm, indicating the main factor that influences the capacity is related to the pores of carbon.

The importance of the mesopore volume of carbon in Li-air batteries can be well explained from the kinetic process, including oxygen diffusion and reduction. During discharge,

oxygen first transports into the whole carbon electrode, either in the gaseous phase or through the electrolyte in the form of dissolved oxygen [354]. However, no matter the oxygen penetration route, the successful formation of  $\text{Li}_2\text{O}_2$  only occurs on the triple junctions where electrolyte, carbon, and oxygen coexist. In other words, the more the tri-phase regions, the more  $\text{Li}_2\text{O}_2$  will be produced and therefore the higher the capacity obtained from the cell. If the pore size is too small and within the micro-size range, the entrance of the micropores will be quickly blocked by either the electrolyte or  $\text{Li}_2\text{O}_2$ , preventing further access to the interior carbon surface. On the other hand, carbons with a large amount of macropores are not suitable for a Li- $\text{O}_2$  battery either because large pores are easily flooded by the electrolyte, reducing the generation of triple junctions. Furthermore, the volumetric energy density of the air electrode will also decrease by macroporous carbons [356]. From this point of view Ketjen black satisfies most of the requirements for the air electrode. Ketjen black is a highly porous carbon with chain-like structure, which determines the porosity of the air electrode prepared from this material. It was postulated that the spring-like structure of Ketjen black expands significantly when soaked in organic electrolyte, which then causes the increase in the porosity of the wetted air electrode [355]. Compared with other carbons, more triple phase reaction points were automatically produced during the expansion process of the porous carbon, facilitating the reaction between  $\text{Li}^+$  and  $\text{O}_2$  while holding more discharge products.

The pore sizes/volume and porosity discussed above are the intrinsic properties of different carbons and can be tuned by various synthesis approaches. A recent interesting work demonstrates that two-dimensional graphene nanosheets without any pores, if manipulated appropriately, can self-assemble into highly porous, 3D architectures with interconnected pore channels [353]. Fig. 22c shows that the functionalized graphene nanosheets aggregate into loosely packed, “broken egg” structures leaving large interconnected tunnels that continue through the entire electrode depth. These tunnels can function as numerous arteries that continuously supply oxygen into the interior of the electrode during the discharge process. It was further revealed, experimentally and theoretically, that  $\text{Li}_2\text{O}_2$  prefers to nucleate and grow near functionalized lattice defect sites on graphene with functional groups as a result of the relatively stronger interaction between the deposited  $\text{Li}_2\text{O}_2$  monomer at the 5-8-5 defects. More importantly, the aggregation of  $\text{Li}_2\text{O}_2$  clusters in the vicinity of those defective sites is

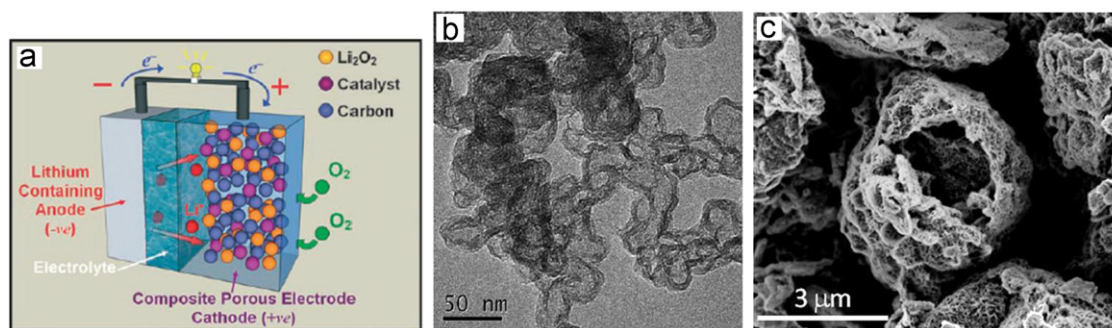


**Figure 22** (a) Schematic representation of a rechargeable Li/ $\text{O}_2$  battery [352], (b) TEM image of Ketjen black EC 300J [183], and (c) SEM image of graphene air electrode [353].

energetically unfavorable; therefore the deposited  $\text{Li}_2\text{O}_2$  would form the isolated nano-sized “islands” on graphene, further ensuring smooth oxygen transport during the discharge process. Limited size or thickness of the reaction products,  $\text{Li}_2\text{O}_2$ , with preferred growth points is important for rechargeable Li-air batteries because it prevents the continuous increase in electrode impedance and improves the efficiency of the cell. Those defects and/or functional groups also provide ideal locations to anchor the catalysts, which then have a constant close contact with  $\text{Li}_2\text{O}_2$  through repeated cycling.

Therefore, a good carbon candidate for Li-air or Li- $\text{O}_2$  batteries should have the characters of accurately controlled pore sizes/volume, which can be performed during synthesis. The surface area of the ideal carbon should also be tailored to reduce the side reactions and reach an optimized performance for the battery. On the other hand, the porous carbon can also be “produced” from non-porous two-dimensional carbons such as graphene nanosheets. The functional groups and/or defects on different porous carbons (not only in graphene) can be modified to satisfy different energy requirements and their interactions with  $\text{Li}_2\text{O}_2$  are an interesting direction that is worth further investigation.

## Summary

There are many ways to make useful graphitic carbon materials, and the structures and functions highly depend on the processing conditions and precursors used. Among these, sol-gel-derived aerogels and cryogels from versatile chemical synthesis routes are widely studied. The porous structure and bulk chemistry of the resulting carbon can be tuned through the selection of precursors, catalysts, and solvents, as well as the through the processing conditions. The surface chemistry and porous structure of carbon can be further manipulated through solvent exchange or chemical impregnation, controlled removal of the solvent, pyrolysis, and activation. With controlled chemistry and porous structure, highly porous carbons demonstrated excellent properties for energy related applications. Porous carbon with tuned porous structure and surface chemistry offered higher specific capacity, better cyclic stability, and potentially higher working voltage when used as electrodes for supercapacitors. It was also demonstrated that porous carbons are a viable media for natural gas storage at reduced pressure. When used as matrices, porous carbons make it possible to fully utilize transition metal oxides as cathodic materials for lithium ion intercalation with enhanced specific power. When hydrides are confined inside pores of highly porous carbon to form coherent nanocomposites, the dehydrogenation temperatures and reaction pathways are both changed significantly: the dehydrogenation temperature and the activation energy decrease with a decreasing pore size, and also change with the surface chemistry of porous carbon.

In the last decade, new structures and forms of carbon have emerged. The best examples include the discovery of fullerenes, and the associated single wall and multi-wall carbon nanotubes. Although atomic and electron level control of carbon nanotubes remains a large scientific and technological challenge, the potential of different kinds of carbon nanotubes and their assemblies for energy storage and conversion has been well demonstrated. In the near future the long term stability of the materials and devices,

as well as the cost of manufacturing of the materials and devices, will be a focal point. In the last few years, another form of carbon, molecularly dispersed graphite, graphene, has attracted wide attention. Graphene not only has unique physical and chemical properties but also provides a great opportunity to understand the fundamental chemical and physical processes involved in the complex systems. Such understanding will be difficult for disordered carbon. However, it is important to keep in mind that although the new carbon materials such as carbon nanotubes and graphene are exciting and may have great potential, they still need to compete with traditional carbon and graphite in terms of cost and performance.

## Acknowledgments

This work has been supported in part by National Science Foundation (DMI-0455994, DMR-0605159, and CMMI-1030048) and Air Force Office of Scientific Research (AFOSR-MURI, FA9550-06-1-0326). This work has also been supported by Washington Technology Center, Pacific Northwest National Laboratory (PNNL), Intel Labs, and EnerG2. SLC acknowledges the University of Washington Bioenergy IGERT fellowship (DGE-0654252) and the GO-MAP fellowship. PNNL researchers would like to acknowledge support from the U.S. Department of Energy (DOE), Office of Basic Energy Sciences, Division of Materials Sciences and Engineering, under Award KC020105-FWP12152. PNNL is a multi-program national laboratory operated for DOE by Battelle under Contract DE-AC05-76RL01830. Tsinghua University researchers acknowledge financial support from National Basic Research Program of China (No. 2011CB935704) and National Natural Science Foundation of China (No. 11079002).

## References

- [1] B.C. Thompson, J.M.J. Frechet, *Angewandte Chemie—International Edition* 47 (2008) 58.
- [2] S.H. Park, et al., *Nature Photonics* 3 (2009) 297.
- [3] H. Spanggaard, F.C. Krebs, *Solar Energy Materials and Solar Cells* 83 (2004) 125.
- [4] G. Dennler, M.C. Scharber, C.J. Brabec, *Advanced Materials* 21 (2009) 1323.
- [5] A.D. Pasquier, H.E. Unalan, A. Kanwal, S. Miller, M. Chhowalla, *Applied Physics Letters* 87 (2005).
- [6] Y.K. Kim, D.H. Min, *Langmuir* 25 (2009) 11302.
- [7] D.S. Hecht, L.B. Hu, G. Irvin, *Advanced Materials* 23 (2011) 1482.
- [8] Y.Q. Sun, Q.O. Wu, G.Q. Shi, *Energy & Environmental Science* 4 (2011) 1113.
- [9] L.L. Zhang, R. Zhou, X.S. Zhao, *Journal of Materials Chemistry* 20 (2010) 5983.
- [10] S.R.C. Vivekchand, C.S. Rout, K.S. Subrahmanyam, A. Govindaraj, C.N.R. Rao, *Journal of Chemical Sciences* 120 (2008) 9.
- [11] K.S. Subrahmanyam, S.R.C. Vivekchand, A. Govindaraj, C.N.R. Rao, *Journal of Materials Chemistry* 18 (2008) 1517.
- [12] E. Frackowiak, F. Beguin, *Carbon* 40 (2002) 1775.
- [13] E. Yoo, et al., *Nano Letters* 8 (2008) 2277.
- [14] Y.P. Wu, E. Rahm, R. Holze, *Journal of Power Sources* 114 (2003) 228.
- [15] B.J. Landi, M.J. Ganter, C.D. Cress, R.A. DiLeo, R.P. Raffaele, *Energy & Environmental Science* 2 (2009) 638.

- [16] H.O. Pierson, *Handbook of Carbon, Graphite, Diamond, and Fullerenes: Properties, Processing, and Applications*, Noyes Publications, Park Ridge, NJ, USA, 1993, pp. xx, 399 p.
- [17] S.R.P. Silva, *Properties of Amorphous Carbon*, INSPEC, London, 2003.
- [18] T. Otowa, Y. Nojima, T. Miyazaki, *Carbon* 35 (1997) 1315.
- [19] C.Y. Lu, H.S. Chiu, *Chemical Engineering Science* 61 (2006) 1138.
- [20] V. Gomez-Serrano, A. Macias-Garcia, A. Espinosa-Mansilla, C. Valenzuela-Calahorro, *Water Research* 32 (1998) 1.
- [21] M.C. Annesini, C. Di Carlo, V. Piemonte, L. Turchetti, *Biochemical Engineering Journal* 40 (205) (2008).
- [22] D.J. Malik, G.L. Warwick, I. Mathieson, N.A. Hoenich, M. Streat, *Carbon* 43 (2005) 2317.
- [23] R.J.A. Bigsby, R.J. Rider, G.N. Blount, *Proceedings of the Institution of Mechanical Engineers Part H—Journal of Engineering in Medicine* 212 (1998) 373.
- [24] C. Ye, Q.M. Gong, F.P. Lu, J. Liang, *Separation and Purification Technology* 58 (2007) 2.
- [25] S.H. Joo, et al., *Nature* 412 (2001) 169.
- [26] E. Auer, A. Freund, J. Pietsch, T. Tacke, *Applied Catalysis A—General* 173 (1998) 259.
- [27] G.G. Park, T.H. Yang, Y.G. Yoon, W.Y. Lee, C.S. Kim, *International Journal of Hydrogen Energy* 28 (2003) 645.
- [28] A. Guha, W.J. Lu, T.A. Zawodzinski, D.A. Schiraldi, *Carbon* 45 (2007) 1506.
- [29] A. Aygun, S. Yenisoay-Karakas, I. Duman, *Microporous and Mesoporous Materials* 66 (2003) 189.
- [30] A. Ahmadvour, D.D. Do, *Carbon* 34 (1996) 471.
- [31] M. Jagtoyen, F. Derbyshire, *Carbon* 36 (1998) 1085.
- [32] Z.H. Hu, M.P. Srinivasan, *Microporous and Mesoporous Materials* 27 (1999) 11.
- [33] M. Ahmedna, W.E. Marshall, R.M. Rao, *Bioresource Technology* 71 (2000) 113.
- [34] D.C. Wu, R.W. Fu, S.T. Zhang, M.S. Dresselhaus, G. Dresselhaus, *Journal of Non-Crystalline Solids* 336 (2004) 26.
- [35] R.W. Pekala, *Journal of Materials Science* 24 (1989) 3221.
- [36] H. Tamon, H. Ishizaka, T. Yamamoto, T. Suzuki, *Carbon* 37 (1999) 2049.
- [37] D. Kawashima, T. Aihara, Y. Kobayashi, T. Kyotani, A. Tomita, *Chemistry of Materials* 12 (2000) 3397.
- [38] N. Job, R. Pirard, J. Marien, J.P. Pirard, *Carbon* 42 (2004) 619.
- [39] C. Lin, J.A. Ritter, *Carbon* 35 (1997) 1271.
- [40] Y. Gogotsi, et al., *Nature Materials* 2 (2003) 591.
- [41] R. Dash, et al., *Carbon* 44 (2006) 2489.
- [42] E. Kockrick, et al., *Carbon* 48 (2010) 1707.
- [43] J.S. Beck, et al., *Journal of the American Chemical Society* 114 (1992) 10834.
- [44] J. Lee, J. Kim, T. Hyeon, *Advanced Materials* 18 (2006) 2073.
- [45] R. Ryoo, S.H. Joo, S. Jun, *Journal of Physical Chemistry B* 103 (1999) 7743.
- [46] J. Lee, S. Yoon, T. Hyeon, S.M. Oh, K.B. Kim, *Chemical Communications* 2177 (1999).
- [47] Hybrid Cars, 2011, <<http://www.hybridcars.com/make/honda-mpg>>, accessed on 7 September 2011.
- [48] AFS Trinity Power Corporation, 2010, <<http://afstrinity.com>>, accessed 7 September 2011.
- [49] Y.H. Kim, *Electronic Component News*, 2002.
- [50] R. Kotz, M. Carlen, *Electrochimica Acta* 45 (2000) 2483.
- [51] E. Frackowiak, *Physical Chemistry Chemical Physics* 9 (2007) 1774.
- [52] F. Pico, et al., *Journal of the Electrochemical Society* 151 (2004) A831.
- [53] E. Frackowiak, K. Metenier, V. Bertagna, F. Beguin, *Applied Physics Letters* 77 (2000) 2421.
- [54] P. Simon, Y. Gogotsi, *Nature Materials* 7 (2008) 845.
- [55] C. Peng, S.W. Zhang, D. Jewell, G.Z. Chen, *Progress in Natural Science—Materials International* 18 (2008) 777.
- [56] A.F. Burke, *Proceedings of the IEEE* 95 (2007) 806.
- [57] V.V.N. Obreja, *Physica E—Low-Dimensional Systems & Nanostructures* 40 (2008) 2596.
- [58] B.E. Conway, *Electrochemical Supercapacitors: Scientific Fundamentals and Technological Applications*, Plenum Press, New York, 1999, pp. xxviii, 698 p.
- [59] A. Garcia-Gomez, P. Miles, T.A. Centeno, J.M. Rojo, *Electrochimica Acta* 55 (2010) 8539.
- [60] E.G. Calvo, C.O. Ania, L. Zubizarreta, J.A. Menendez, A. Arenillas, *Energy & Fuels* 24 (2010) 3334.
- [61] A. Szczurek, et al., *Carbon* 48 (2010) 3874.
- [62] M. Inagaki, H. Konno, O. Tanaiki, *Journal of Power Sources* 195 (2010) 7880.
- [63] W. Feng, X. Bin, *New Carbon Materials* 21 (2006) 176.
- [64] J.H. Chen, et al., *Carbon* 40 (2002) 1193.
- [65] J.N. Barisci, G.G. Wallace, R.H. Baughman, *Journal of Electroanalytical Chemistry* 488 (2000) 92.
- [66] M.W. Xu, D.D. Zhao, S.J. Bao, H.L. Li, *Journal of Solid State Electrochemistry* 11 (2007) 1101.
- [67] S. Yamazaki, K. Obata, Y. Okuhama, Y. Matsuda, M. Ishikawa, *Electrochemistry* 75 (2007) 592.
- [68] A.L.M. Reddy, S. Ramaprabhu, *Journal of Physical Chemistry C* 111 (2007) 7727.
- [69] K. Jurewicz, S. Delpeux, V. Bertagna, F. Beguin, E. Frackowiak, *Chemical Physics Letters* 347 (2001) 36.
- [70] A.E. Fischer, K.A. Pettigrew, D.R. Rolison, R.M. Stroud, J.W. Long, *Nano Letters* 7 (2007) 281.
- [71] E. Raymundo-Pinero, V. Khomenko, E. Frackowiak, F. Beguin, *Journal of the Electrochemical Society* 152 (2005) A229.
- [72] E. Frackowiak, V. Khomenko, K. Jurewicz, K. Lota, F. Beguin, *Journal of Power Sources* 153 (2006) 413.
- [73] V. Khomenko, E. Raymundo-Pinero, F. Beguin, *Journal of Power Sources* 153 (2006) 183.
- [74] S. Sepehri, B.B. Garcia, Q.F. Zhang, G.Z. Cao, *Carbon* 47 (2009) 1436.
- [75] B.B. Garcia, et al., *Journal of Applied Physics* 104 (2008).
- [76] T. Yamamoto, T. Nishimura, T. Suzuki, H. Tamon, *Journal of Non-Crystalline Solids* 288 (2001) 46.
- [77] J.G. Lee, J.Y. Kim, S.H. Kim, *Journal of Power Sources* 160 (2006) 1495.
- [78] J. Chmiola, et al., *Science* 313 (2006) 1760.
- [79] V. Presser, M. Heon, Y. Gogotsi, *Advanced Functional Materials* 21 (2011) 810.
- [80] M. Rose, E. Kockrick, I. Senkovska, S. Kaskel, *Carbon* 48 (2010) 403.
- [81] J. Chmiola, G. Yushin, R. Dash, Y. Gogotsi, *Journal of Power Sources* 158 (2006) 765.
- [82] V. Presser, et al., *Advanced Energy Materials* 1 (2011) 423.
- [83] C. Liang, Z. Li, S. Dai, *Angewandte Chemie—International Edition* 47 (2008) 3696.
- [84] Y. Shi, Y. Wan, D. Zhao, *Chemical Society Reviews* 40 (2011) 3854.
- [85] C. Niu, E.K. Sichel, R. Hoch, D. Moy, H. Tennent, *Applied Physics Letters* 70 (1997) 1480.
- [86] R.Z. Ma, et al., *Journal of Power Sources* 84 (1999) 126.
- [87] J.H. Kim, K.W. Nam, S.B. Ma, K.B. Kim, *Carbon* 44 (2006) 1963.
- [88] K.H. An, et al., *Advanced Materials* 13 (2001) 497.
- [89] C. Vix-Guterl, et al., *Carbon* 43 (2005) 1293.
- [90] C.G. Liu, H.T. Fang, F. Li, M. Liu, H.M. Cheng, *Journal of Power Sources* 160 (2006) 758.
- [91] A.B. Fuertes, F. Pico, J.M. Rojo, *Journal of Power Sources* 133 (2004) 329.
- [92] B.J. Yoon, et al., *Chemical Physics Letters* 388 (2004) 170.
- [93] Z.P. Huang, et al., *Applied Physics Letters* 73 (1998) 3845.
- [94] E. Frackowiak, F. Béguin, *Carbon* 39 (2001) 937.
- [95] A.G. Pandolfo, A.F. Hollenkamp, *Journal of Power Sources* 157 (2006) 11.

- [96] P. Azais, et al., *Journal of Power Sources* 171 (2007) 1046.
- [97] D.N. Futaba, et al., *Nature Materials* 5 (2006) 987.
- [98] A.K. Shukla, S. Sampath, K. Vijayamohan, *Current Science* 79 (2007) 1656.
- [99] D.N. Futaba, et al., *Nature Materials* 5 (2006) 987.
- [100] C. Du, J. Yeh, N. Pan, *Nanotechnology* 16 (2005) 350.
- [101] L. Gao, et al., *Solid State Communications* 146 (2008) 380.
- [102] C. Emmenegger, et al., *Carbon* 41 (2003) 539.
- [103] M. Kaempgen, J. Ma, G. Gruner, G. Wee, S.G. Mhaisalkar, *Applied Physics Letters* 90 (2007) 264104.
- [104] A.L.M. Reddy, M.M. Shaijumon, S.R. Gowda, P.M. Ajayan, *Journal of Physical Chemistry C* 114 (2010) 658.
- [105] V.L. Pushparaj, et al., *PNAS* 104 (2007) 13574.
- [106] X. Qin, S. Durbach, G.T. Wu, *Carbon* 42 (2004) 451.
- [107] J.Y. Lee, K. Liang, K.H. An, Y.H. Lee, *Synthetic Methods* 150 (2005) 153.
- [108] P.-C. Chen, G. Shen, S. Sukcharoenchoke, C. Zhou, *Applied Physics Letters* 94 (2009) 043113.
- [109] K.H. An, et al., *Journal of Electrochemical Society* 149 (2002) A1058.
- [110] V. Gupta, N. Miura, *Electrochimica Acta* 52 (2006) 1721.
- [111] J. Zhang, L.-B. Kong, B. Wang, Y.-C. Luo, L. Kang, *Synthetic Methods* 159 (2009) 260.
- [112] H.T. Liu, P. He, Z.Y. Li, Y. Liu, J.H. Li, *Electrochimica Acta* 51 (2006) 1925.
- [113] V. Gupta, N. Miura, *Materials Letters* 60 (2006) 1466.
- [114] L.Z. Fan, J. Maier, *Electrochemical Communications* 8 (2006) 937.
- [115] J. Yana, et al., *Journal of Power Sources* 194 (2009) 1202.
- [116] Q. Wang, Z.H. Wen, J.H. Li, *Advanced Functional Materials* 16 (2006) 2141.
- [117] S.D. Meryl, P. Sungjin, Z. Yanwu, A. Jinho, R.S. Rodney, *Nano Letters* 8 (2008) 3498.
- [118] S.R.C. Vivekchand, C.S. Rout, K.S. Subrahmanyam, A. Govindaraj, C.N.R. Rao, *Journal of Chemical Science* 120 (2008) 9.
- [119] A. Yu, I. Roes, A. Davies, Z. Chen, *Applied Physics Letters* 96 (2010) 253105.
- [120] Y. Wang, et al., *Journal of Physical Chemistry C* 113 (2009) 13103.
- [121] C. Liu, Z. Yu, D. Neff, A. Zhamu, B.Z. Jang, *Nano Letters* 10 (2010) 4863.
- [122] J. Xu, K. Wang, S.-Z. Zu, B.-H. Han, Z. Wei, *ACS Nano* 4 (2010) 5019.
- [123] L.L. Zhang, S. Zhao, X.N. Tian, X.S. Zhao, *Langmuir* 26 (2010) 17624.
- [124] K. Zhang, L.L. Zhang, X.S. Zhao, J. Wu, *Chemical Materials* 22 (2010) 1392.
- [125] D.-W. Wang, et al., *ACS Nano* 3 (2009) 1745.
- [126] H. Gómez, et al., *Journal of Power Sources* 196 (2011) 4102.
- [127] J. Yan, et al., *Journal of Power Sources* 195 (2010) 3041.
- [128] D.-S. Yu, L.-M. Dai, *Journal of Physical Chemistry Letters* 1 (2010) 467.
- [129] S. Wang, S.P. Jiang, X. Wang, *Electrochimica Acta* 56 (2011) 3338.
- [130] L.L. Zhang, T. Wei, W. Wang, X.S. Zhao, *Microporous and Mesoporous Materials* 123 (2009) 260.
- [131] J. Jiang, et al., *Applied Materials Interfaces* 3 (2011) 99.
- [132] H. Wang, H.S. Casalongue, Y. Liang, H. Dai, *Journal of American Chemical Society* 132 (2010) 7472.
- [133] C. Yuan, et al., *Materials Letters* 65 (2011) 374.
- [134] J. Yan, et al., *Carbon* 48 (2010) 3825.
- [135] H. Zhang, X. Lv, Y. Li, Y. Wang, J.H. Li, *ACS Nano* 4 (2009) 380.
- [136] Y.M. Li, L.H. Tang, J.H. Li, *Electrochemical Communications* 11 (2009) 846.
- [137] H.X. Chang, X. Lv, H. Zhang, J.H. Li, *Electrochemical Communications* 12 (2010) 483.
- [138] Y. Wang, Y. Shao, D.W. Matson, J.H. Li, Y.H. Lin, *ACS Nano* 4 (2010) 1790.
- [139] Y. Wang, Y. Li, L. Tang, J. Lu, J.H. Li, *Electrochemical Communications* 11 (2009) 889.
- [140] Y. Wang, J. Lu, L.H. Tang, H.X. Chang, J.H. Li, *Analytical Chemistry* 81 (2009).
- [141] H.X. Chang, L.H. Tang, Y. Wang, J.H. Jiang, J.H. Li, *Analytical Chemistry* 82 (2010) 2341.
- [142] X.L. Dong, J.S. Cheng, J.H. Li, Y.S. Wang, *Analytical Chemistry* 82 (2010) 6208.
- [143] L.H. Tang, H.B. Feng, J.S. Cheng, J.H. Li, *Chemical Communications* 46 (2010) 5882.
- [144] F. Chen, Q. Qing, J. Xia, J.H. Li, N.J. Tao, *Journal of American Chemical Society* 131 (2009) 9908.
- [145] Y. Wang, et al., *Journal of American Chemical Society* 132 (2010) 9274.
- [146] J.M. Tarascon, M. Armand, *Nature* 414 (2001) 359.
- [147] J. Hassoun, P. Reale, B. Scrosati, *Journal of Materials Chemistry* 17 (2007) 3668.
- [148] M. Armand, J.M. Tarascon, *Nature* 451 (2008) 652.
- [149] L. Taberna, S. Mitra, P. Poizot, P. Simon, J.M. Tarascon, *Nature Materials* 5 (2006) 567.
- [150] W. Rudorff, U. Hofmann, *Zeitschrift Fur Anorganische Und Allgemeine Chemie* 238 (1938) 1.
- [151] M. Armand, P. Touzain, *Materials Science and Engineering* 31 (1977) 319.
- [152] N.A. Kaskhedikar, J. Maier, *Advanced Materials* 21 (2009) 2664.
- [153] K. Sato, M. Noguchi, A. Demachi, N. Oki, M. Endo, *Science* 264 (1994) 556.
- [154] T. Zheng, J.N. Reimers, J.R. Dahn, *Physical Review B* 51 (1995) 734.
- [155] J.R. Dahn, T. Zheng, Y.H. Liu, J.S. Xue, *Science* 270 (1995) 590.
- [156] T. Zheng, et al., *Journal of the Electrochemical Society* 142 (1995) 2581.
- [157] T. Zheng, Q. Zhong, J.R. Dahn, *Journal of the Electrochemical Society* 142 (1995) L211.
- [158] J.M. Tarascon, M. Armand, *Nature* 414 (2001) 359.
- [159] A.S. Claye, J.E. Fischer, C.B. Huffman, A.G. Rinzler, R.E. Smalley, *Journal of Electrochemical Society* 147 (2000) 2845.
- [160] J.N. Barisci, G.C. Wallace, R.H. Baughman, *Electrochimica Acta* 46 (2000) 509.
- [161] J. Zhao, A. Buldum, J. Han, J.P. Lu, *Physics Review Letters* 85 (2000) 1706.
- [162] G.T. Wu, et al., *Journal of Power Sources* 75 (1998) 175.
- [163] S.Y. Chew, et al., *Carbon* 47 (2009) 2976.
- [164] E. Frackowiak, S. Gautier, H. Gaucher, S. Bonnamy, F. Beguin, *Carbon* 37 (1999) 61.
- [165] B. Gao, et al., *Chemical Physics Letters* 327 (2000) 69.
- [166] H. Shimoda, et al., *Physics Review Letters* 88 (2002) 015502.
- [167] J. Zhao, Q.Y. Gao, C. Gu, Y. Yang, *Chemical Physics Letters* 358 (2002) 77.
- [168] H. Zhang, et al., *Electrochimica Acta* 55 (2010) 2873.
- [169] G.L. Che, B.B. Lakshmi, E.R. Fisher, C.R. Martin, *Nature* 393 (1998) 346.
- [170] W.X. Chen, J.Y. Lee, Z.L. Liu, *Carbon* 41 (2003) 959.
- [171] W. Wang, P.N. Kumta, *ACS Nano* 4 (2010) 2233.
- [172] Y.M. Li, X.J. Lv, J. Lu, J.H. Li, *Journal of Physical Chemistry C* 114 (2010) 21770.
- [173] L. Cui, Y. Yang, C. Hsu, Y. Cui, *Nano Letters* 9 (2009) 3370.
- [174] Y. Zhao, J.X. Li, Y.H. Ding, L.H. Guan, *Chemical Communications* 47 (2011) 7416.
- [175] H. Xia, M.O. Lai, L. Lu, *Journal of Materials Chemistry* 20 (2010) 6896.
- [176] Y. Nuli, J. Yang, M.S. Jiang, *Materials Letters* 62 (2008) 2092.
- [177] J.T. Yin, et al., *Journal of Electrochemical Society* 152 (2005) A1341.

- [178] L.Y. Beaulieu, J.R. Dahn, *Journal of Electrochemical Society* 147 (2000) 3237.
- [179] O. Mao, J.R. Dahn, *Journal of Electrochemical Society* 146 (1999) 423.
- [180] Y.-S. He, et al., *Electrochemical Communications* 12 (2010) 570.
- [181] S.F. Zheng, et al., *Chemical Materials* 20 (2008) 3617.
- [182] H. Li, Q. Wang, L. Shi, L. Chen, X. Huang, *Chemical Materials* 14 (2002) 103.
- [183] Z. Wang, G. Chen, D. Xia, *Journal of Power Sources* 184 (2008) 432.
- [184] T.P. Kumar, R. Ramesh, Y.Y. Lin, G.T. Fey, *Electrochemical Communications* 6 (2004) 520.
- [185] A.L.M. Reddy, M.M. Shaijumon, S.R. Gowda, P.M. Ajayan, *Nano Letters* 9 (2009) 1002.
- [186] L.F. Cui, L. Hu, J.W. Choi, Y. Cui, *ACS Nano* 4 (2010) 3671.
- [187] Q. Wang, J.H. Li, *Journal of Physical Chemistry C* 111 (2007) 1675.
- [188] S.H. Ng, et al., *Electrochimica Acta* 51 (2005) 23.
- [189] A. Kiebele, G. Gruner, *Applied Physics Letters* 91 (2007) 144104.
- [190] J. Chen, et al., *Chemical Materials* 19 (2007).
- [191] W. Wang, R. Epur, P.N. Kumta, *Electrochemical Communications* 13 (2011) 429.
- [192] K.S. Novoselov, et al., *Science* 306 (2004) 666.
- [193] Y.B. Zhang, Y.W. Tan, H.L. Stomer, P. Kim, *Nature* 438 (2005) 201.
- [194] A. Altland, *Physics Review Letters* 97 (2006) 236802.
- [195] D. Chen, L.H. Tang, J.H. Li, *Chem. Soc. Rev.* 39 (2010) 3157.
- [196] D.A.C. Brownson, D.K. Kampouris, *Journal of Power Sources* 196 (2011) 4873.
- [197] M. Pumera, *Energy Environmental Science* 4 (2011) 668.
- [198] P. Lian, et al., *Electrochimica Acta* 55 (2010) 3909.
- [199] D. Pan, et al., *Chemical Materials* 21 (2009) 3136.
- [200] L.-J. Fu, et al., *Solid State Science* 8 (2006) 113.
- [201] T. Bhardwaj, A. Antic, B. Pavan, V. Barone, B.D. Fahlman, *Journal of American Chemical Society* 132 (2010) 12556.
- [202] S. Yin, et al., *ACS Nano* 5 (2011) 3831.
- [203] Z.-S. Wu, et al., *ACS Nano* 3187 (2010).
- [204] D. Wang, et al., *ACS Nano* 3 (2009) 907.
- [205] X. Zhu, Y. Zhu, S. Murali, M.D. Stoller, R.S. Ruoff, *ACS Nano* 5 (2011) 3333.
- [206] G. Zhou, et al., *Chemical Materials* 22 (2010) 5306.
- [207] H. Wang, et al., *Journal of American Chemical Society* 13978 (2010).
- [208] G. Wang, J. Bai, Y. Wang, Z. Rena, J. Bai, *Scripta Materials* 65 (2011) 339.
- [209] Y.J. Mai, et al., *Electrochimica Acta* 56 (2011) 2306.
- [210] J. Zhu, et al., *Nanoscale* 3 (2011) 1084.
- [211] H. Xiang, et al., *Carbon* 49 (2011) 1787.
- [212] H. Kim, et al., *Journal of Electrochemical Society* 158 (2011) A930.
- [213] S. Chen, P. Chen, M. Wu, D. Pan, Y. Wang, *Electrochemical Communications* 12 (2010) 1302.
- [214] Z.-J. Fan, et al., *ACS Nano* 5 (2011) 2787.
- [215] J.-Z. Wang, et al., *Chemical European Journal* 17 (2011) 661.
- [216] E. Yoo, et al., *Nano Letters* 8 (2008) 2277.
- [217] T.P. McNicholas, et al., *Journal of Physical Chemistry C* 114 (2010) 13902.
- [218] C. Guan, K. Wang, C. Yang, X.S. Zhao, *Microporous and Mesoporous Materials* 118 (2009) 503.
- [219] K.S. Xia, Q.M. Gao, C.D. Wu, S.Q. Song, M.L. Ruan, *Carbon* 45 (2007) 1989.
- [220] Z.X. Yang, Y.D. Xia, R. Mokaya, *Journal of the American Chemical Society* 129 (2007) 1673.
- [221] B. Panella, M. Hirscher, S. Roth, *Carbon* 43 (2005) 2209.
- [222] A. Feaver, G.Z. Cao, *Carbon* 44 (2006) 590.
- [223] K.M. Thomas, *Catalysis Today* 120 (2007) 389.
- [224] A. Chambers, C. Park, R.T.K. Baker, N.M. Rodriguez, *Journal of Physical Chemistry B* 102 (1998) 4253.
- [225] A.C. Dillon, et al., *Nature* 386 (1997) 377.
- [226] Q.Y. Wang, J.K. Johnson, *Journal of Physical Chemistry B* 103 (1999) 277.
- [227] A. Zuttel, *Naturwissenschaften* 91 (2004) 157.
- [228] P. Kowalczyk, R. Holyst, M. Terrones, H. Terrones, *Physical Chemistry Chemical Physics* 9 (2007) 1786.
- [229] R. Stobel, J. Garche, P.T. Moseley, L. Jorissen, G. Wolf, *Journal of Power Sources* 159 (2006) 781.
- [230] H.G. Schimmel, et al., *Chemistry—A European Journal* 9 (2003) 4764.
- [231] L. Zhou, Y.P. Zhou, Y. Sun, *International Journal of Hydrogen Energy* 29 (2004) 319.
- [232] A. Zuttel, et al., *International Journal of Hydrogen Energy* 27 (2002) 203.
- [233] H. Kabbour, T.F. Baumann, J.H. Satcher, A. Saulnier, C.C. Ahn, *Chemistry of Materials* 18 (2006) 6085.
- [234] T.C.M. Chung, Y. Jeong, Q. Chen, A. Kleinhammes, Y. Wu, *Journal of the American Chemical Society* 130 (2008) 6668.
- [235] E. Kennedy, *The Fresno Bee* (2005).
- [236] N.G.V.f. America, 2011.
- [237] S. Biloe, V. Goetz, A. Guillot, *Carbon* 40 (2002) 1295.
- [238] T. Duren, L. Sarkisov, O.M. Yaghi, R.Q. Snurr, *Langmuir* 20 (2004) 2683.
- [239] A. Perrin, A. Celzard, J.F. Mareche, G. Furdin, *Energy & Fuels* 17 (2003) 1283.
- [240] A.C. Lua, T. Yang, *Carbon* 42 (2004) 224.
- [241] T. Yang, A.C. Lua, *Microporous and Mesoporous Materials* 63 (2003) 113.
- [242] A.C. Lua, T. Yang, *Journal of Colloid and Interface Science* 274 (2004) 594.
- [243] A.C. Lua, T. Yang, J. Guo, *Journal of Analytical and Applied Pyrolysis* 72 (2004) 279.
- [244] J. Alcaniz-Monge, M.A. De La Casa-Lillo, C. Cazorla-Amoros, A. Linares-Solano, *Carbon* 35 (1997) 291.
- [245] T.A. Brady, M. RostamAbadi, M.J. Rood, *Gas Separation & Purification* 10 (1996) 97.
- [246] Y.S. Hsu, T.P. Perng, *Journal of Alloys and Compounds* 227 (1995) 180.
- [247] K. Inomata, K. Kanazawa, Y. Urabe, H. Hosono, T. Araki, *Carbon* 40 (2002) 87.
- [248] B. Fang, Y.Z. Wei, K. Maruyama, M. Kumagai, *Journal of Applied Electrochemistry* 35 (2005) 229.
- [249] A.F. Gross, C.C. Ahn, S.L. Van Atta, P. Liu, J.J. Vajo, *Nanotechnology* 20 (2009).
- [250] R.W. Pekala, D.W. Schaefer, *Macromolecules* 26 (1993) 5487.
- [251] H. Tamon, H. Ishizaka, M. Mikami, M. Okazaki, *Carbon* 35 (1997) 791.
- [252] C. Schmitt, H. Probstle, J. Fricke, *Journal of Non-Crystalline Solids* 285 (2001) 277.
- [253] V.P. Utgikar, *Technology in Society* 27 (2005) 315.
- [254] J.F. Hake, J. Linssen, M. Walbeck, *Energy Policy* 34 (2006) 1271.
- [255] W. Grochala, P.P. Edwards, *Chemical Reviews* 104 (2004) 1283.
- [256] J. Biener, et al., *Energy & Environmental Science* 4 (2011) 656.
- [257] C.Z. Wu, H.M. Cheng, *Journal of Materials Chemistry* 20 (2010) 5390.
- [258] S. Cahen, J.B. Eymery, R. Janot, J.M. Tarascon, *Journal of Power Sources* 189 (2009) 902.
- [259] L. Li, et al., *Advanced Functional Materials* 19 (2009) 265.
- [260] A.F. Gross, J.J. Vajo, S.L. Van Atta, G.L. Olson, *Journal of Physical Chemistry C* 112 (2008) 5651.
- [261] A. Feaver, et al., *Journal of Physical Chemistry B* 111 (2007) 7469.
- [262] S. Sepehri, B.B. Garcia, G.Z. Cao, *Journal of Materials Chemistry* 18 (2008) 4034.

- [263] F. Baitalow, J. Baumann, G. Wolf, K. Jaenicke-Rossler, G. Leitner, *Thermochimica Acta* 391 (2002) 159.
- [264] A. Gutowska, et al., *Angewandte Chemie-International Edition* 44 (2005) 3578.
- [265] S. Sepehri, et al., *Journal of Physical Chemistry B* 111 (2007) 14285.
- [266] H.E. Kissinger, *Analytical Chemistry* 29 (1957) 1702.
- [267] S. Sepehri, B.B. Garcia, G.Z. Cao, *European Journal of Inorganic Chemistry* 599 (2009).
- [268] T.B. Marder, *Angewandte Chemie—International Edition* 46 (2007) 8116.
- [269] F.H. Stephens, V. Pons, R.T. Baker, *Dalton Transactions* 2613 (2007).
- [270] A.L. Dicks, *Journal of Power Sources* 156 (2006) 128.
- [271] E. Antolini, *Applied Catalysis B—Environmental* 88 (2009) 1.
- [272] Y.Y. Shao, J. Liu, Y. Wang, Y.H. Lin, *Journal of Materials Chemistry* 19 (2009) 46.
- [273] H.S. Liu, et al., *Journal of Power Sources* 155 (2006) 95.
- [274] K.P. Gong, F. Du, Z.H. Xia, M. Durstock, L.M. Dai, *Science* 323 (2009) 760.
- [275] Y.Y. Shao, J.H. Sui, G.P. Yin, Y.Z. Gao, *Applied Catalysis B—Environmental* 79 (2008) 89.
- [276] F. Jaouen, et al., *Energy & Environmental Science* 4 (2011) 114.
- [277] S. Litster, G. McLean, *Journal of Power Sources* 130 (2004) 61.
- [278] V. Mehta, J.S. Cooper, *Journal of Power Sources* 114 (2003) 32.
- [279] R. Kannan, B.A. Kakade, V.K. Pillai, *Angewandte Chemie—International Edition* 47 (2008) 2653.
- [280] E. Yoo, et al., *Nano Letters* 9 (2009) 2255.
- [281] J.G. Zhou, et al., *Chemical Physics Letters* 437 (2007) 229.
- [282] Y.K. Zhou, et al., *Energy & Environmental Science* 3 (2010) 1437.
- [283] Y.Y. Shao, G.P. Yin, J.J. Wang, Y.Z. Gao, P.F. Shi, *Journal of Power Sources* 161 (2006) 47.
- [284] W.Z. Li, et al., *Journal of Physical Chemistry B* 107 (2003) 6292.
- [285] C. Wang, et al., *Nano Letters* 4 (2004) 345.
- [286] Y.Y. Shao, G.P. Yin, Y.Z. Gao, P.F. Shi, *Journal of the Electrochemical Society* 153 (2006) A1093.
- [287] G. Wu, B.Q. Xu, *Journal of Power Sources* 174 (2007) 148.
- [288] Y.W. Tang, S. Cao, Y. Chen, J.C. Bao, T.H. Lu, *Chemical Journal of Chinese Universities—Chinese* 28 (2007) 936.
- [289] W.Z. Li, X. Wang, Z.W. Chen, M. Waje, Y.S. Yan, *Journal of Physical Chemistry B* 110 (2006) 15353.
- [290] Z. Chen, W. Deng, X. Wang, Y. Yan, *ECS Transactions* 11 (2007) 1289.
- [291] E. Yoo, T. Okada, T. Kizuka, J. Nakamura, *Electrochemistry* 75 (2007) 146.
- [292] E.S. Steigerwalt, G.A. Deluga, C.M. Lukehart, *Journal of Physical Chemistry B* 106 (2002) 760.
- [293] S. Shanmugam, A. Gedanken, *Electrochemistry Communications* 8 (2006) 1099.
- [294] Y.Y. Shao, et al., *Journal of Nanoscience and Nanotechnology* 9 (2009) 5811.
- [295] F. Kurusu, et al., *Analyst* 131 (2006) 1292.
- [296] P.J. Britto, K.S.V. Santhanam, A. Rubio, J.A. Alonso, P.M. Ajayan, *Advanced Materials* 11 (1999) 154.
- [297] F.B. Su, et al., *Chemistry of Materials* 17 (2005) 3960.
- [298] W.C. Choi, et al., *Advanced Materials* 17 (2005) 446.
- [299] G.S. Chai, S.B. Yoon, J.S. Yu, J.H. Choi, Y.E. Sung, *Journal of Physical Chemistry B* 108 (2004) 7074.
- [300] G.L. Che, B.B. Lakshmi, E.R. Fisher, C.R. Martin, *Nature* 393 (1998) 346.
- [301] Z.H. Wen, J. Liu, J.H. Li, *Advanced Materials* 20 (2008) 743.
- [302] H. Chang, S.H. Joo, C. Pak, *Journal of Materials Chemistry* 17 (2007) 3078.
- [303] J.S. Yu, S. Kang, S.B. Yoon, G. Chai, *Journal of the American Chemical Society* 124 (2002) 9382.
- [304] H.D. Du, et al., *Journal of Physical Chemistry C* 111 (2007) 2040.
- [305] R. Kou, et al., *Journal of the American Chemical Society* 133 (2011) 2541.
- [306] R. Kou, et al., *Electrochemistry Communications* 11 (2009) 954.
- [307] Y.Y. Shao, et al., *Journal of Power Sources* 195 (2010) 1805.
- [308] G. Gupta, et al., *Chemistry of Materials* 21 (2009) 4515.
- [309] D.A. Stevens, M.T. Hicks, G.M. Haugen, J.R. Dahn, *Journal of the Electrochemical Society* 152 (2005) A2309.
- [310] M. Lefevre, E. Proietti, F. Jaouen, J.P. Dodelet, *Science* 324 (2009) 71.
- [311] G. Wu, K.L. More, C.M. Johnston, P. Zelenay, *Science* 332 (2011) 443.
- [312] H. Chang, H. Zhang, X. Lv, J. Li, *Electrochemical Communications* 12 (2010) 483.
- [313] I. Ahmad, U. Khanb, Y.K. Gun'ko, *Journal of Material Chemistry* 21 (2011) 16990.
- [314] A.K.K. Kyaw, et al., *Applied Physics Letters* 99 (2011) 021107.
- [315] J. Yu, J. Fan, B. Cheng, *Journal of Power Sources* 196 (2011) 7891.
- [316] J. Wei, et al., *Nano Letters* 7 (2007) 2317.
- [317] E. Ramasamy, J. Chun, J. Lee, *Carbon* 48 (2010) 4556.
- [318] B. Fang, et al., *Journal of Materials Chemistry* 21 (2011) 8742.
- [319] M.A. Contreras, et al., *Journal of Physical Chemistry C* 111 (2007) 14045.
- [320] T. Chen, et al., *Angewandte Chemical International Edition* 50 (2011) 1815.
- [321] L.J. Brennan, M.T. Byrne, M. Bari, Y.K. Gun'ko, *Advanced Energy Materials* 1 (2011) 472.
- [322] A. Mathew, G.M. Rao, N. Munichandraiah, *Materials Research Bulletin* 46 (2011) 2045.
- [323] T. Charinpanitkul, et al., *Materials Research Bulletin* 46 (2011) 1604.
- [324] X.L.J. Zhang, W. Guo, T. Hreida, J. Houc, H. Sua, Z. Yuan, *Electrochimica Acta* 56 (2011) 3147.
- [325] H. Chang, Y. Liu, H. Zhang, J. Li, *Journal of Electroanalytical Chemistry* 656 (2011) 269.
- [326] G. Zhu, L. Pan, T. Lu, T. Xu, Z. Sun, *Journal of Materials Chemistry* 21 (2011) 14869.
- [327] H. Zhang, X. Lv, Y. Li, L. Li, J. Li, *ACS Nano* 4 (2010) 380.
- [328] G. Li, F. Wang, Q. Jiang, X. Gao, P. Shen, *Angewandte Chemical International Edition* 49 (2010) 3653.
- [329] P. Dong, et al., *ACS Applied Materials Interfaces* 3 (2011) 3157.
- [330] S. Li, et al., *Advanced Energy Materials* 486 (2011).
- [331] K.S. Lee, W.J. Lee, N.-G. Park, S.O. Kim, J.H. Park, *Chemical Communications* 47 (2011) 4264.
- [332] H. Zhou, et al., *Advanced Materials* 21 (2009) 3919.
- [333] P.-L. Ong, W.B. Euler, I.A. Levitsky, *Nanotechnology* 21 (2010) 105203.
- [334] G. Kalita, et al., *Journal of Physics D: Applied Physics* 42 (2009) 115104.
- [335] Q. Shu, et al., *Nano Letters* 9 (2009) 4338.
- [336] Y. Jia, et al., *Nano Letters* 11 (2011) 1901.
- [337] Y. Jia, et al., *Applied Physics Letters* 98 (2011) 133115.
- [338] R.D. Rauh, K.M. Abraham, G.F. Pearson, J.K. Surprenant, S.B. Brummer, *Journal of the Electrochemical Society* 126 (1979) 523.
- [339] J. Shim, K.A. Striebel, E.J. Cairns, *Journal of the Electrochemical Society* 149 (2002) A1321.
- [340] D. Peramunage, S. Licht, *Science* 261 (1993) 1029.
- [341] V.S. Kolosnitsyn, A.M. Skundin, *Russian Journal of Electrochemistry* 44 (2008) 505.
- [342] C. Liang, N.J. Dudney, J.Y. Howe, *Chemistry of Materials* 21 (2009) 4724.
- [343] N. Jayaprakash, J. Shen, S.S. Moganty, A. Corona, L.A. Archer, *Angewandte Chemie—International Edition* 50, 5904 (2011).

- [344] X. Ji, K.T. Lee, L.F. Nazar, *Nature Materials* 8 (2009) 500.
- [345] Y.C. Xiaolin Li, Wen Qi, Laxmikant V. Saraf, Jie Xiao, a Zimin Nie, Jaroniec Mietek, Ji-Guang Zhang, Birgit Schwenzer, Jun Liu, *Journal of Materials Chemistry* (2011).
- [346] Y. Cao, et al., *Physical Chemistry Chemical Physics* 13 (2011) 7660.
- [347] J.-S. Lee, et al., *Advanced Energy Materials* 1 (2011) 34.
- [348] Y.-C. Lu, H.A. Gasteiger, M.C. Parent, V. Chiloyan, Y. Shao-Horn, *Electrochemical and Solid State Letters* 13 (2010) A69.
- [349] J. Read, et al., *Journal of the Electrochemical Society* 150 (2003) A1351.
- [350] A. Debart, A.J. Paterson, J. Bao, P.G. Bruce, *Angewandte Chemie—International Edition* 47 (2008) 4521.
- [351] S.S. Zhang, D. Foster, J. Read, *Journal of Power Sources* 195 (2010) 1235.
- [352] J. Xiao, et al., *Journal of the Electrochemical Society* 157 (2010) A487.
- [353] D.M. Jie Xiao, Xiaolin Li, Wu Xu, Deyu Wang, Gordon L. Graff, Wendy D. Bennett, Zimin Nie, Laxmikant V. Saraf, Ilhan A. Aksay, Jun Liu, Ji-Guang Zhang, *Nano Letters* (2011).
- [354] X.-H. Yang, P. He, Y.-y. Xia, *Electrochemistry Communications* 11 (2009) 1127.
- [355] T. Kuboki, T. Okuyama, T. Ohsaki, N. Takami, *Journal of Power Sources* 146 (2005) 766.
- [356] G. Wang, et al., *Journal of Power Sources* 180 (2008) 176.



**Dr. Jun Liu** is a Laboratory Fellow at the Pacific Northwest National Laboratories, and leader for the Transformational Materials Science Initiative. Dr. Liu's main research interest includes synthesis of functional nanomaterials for energy storage, catalysis, environmental separation and health care. He has received a R&D 100 Award, two BES Awards, and was named 2007 Distinguished Inventor of Battelle, and is an AAAS fellow. He has over 270 publications.



**Jinghong Li** is currently a Cheung Kong Professor in the Department of Chemistry at Tsinghua University, China. His current research interests include electroanalytical chemistry, bioelectrochemistry and sensors, physical electrochemistry and interfacial electrochemistry, material electrochemistry and power sources. He has published over 250 papers in international, peer-reviewed journals with >10 invited review articles, the citations of which exceed 5500, giving him an h-index of 44.



**Dr. Guozhong Cao** is a Boeing–Steiner Professor of Materials Science and Engineering, Professor of Chemical Engineering, and Adjunct Professor of Mechanical Engineering at the University of Washington. He has published over 280 papers, 7 books and 4 proceedings. His recent research is focused mainly on solar cells, lithium-ion batteries, supercapacitors, and hydrogen storage.



**Stephanie L. Candelaria** is pursuing Ph.D. in the Department of Materials Science and Engineering at the University of Washington under the direction of Professor Guozhong Cao. Her current research is focused on the sol-gel processing and electrochemical characterization of highly porous carbon from renewable resources for supercapacitors.